J. exp. Biol. 117, 251–269 (1985)
Printed in Great Britain © *The Company of Biologists Limited 1985*

THE NEURAL BASIS OF ESCAPE SWIMMING BEHAVIOUR IN THE SQUAT LOBSTER *GALATHEA STRIGOSA*

I. ABSENCE OF CORD GIANT AXONS AND ANATOMY OF MOTOR NEURONES INVOLVED IN SWIMMING

BY KEITH T. SILLAR* AND WILLIAM J. HEITLER

Gatty Marine Laboratory and Department of Zoology, University of St Andrews, St Andrews, Fife, KY16 8LB, Scotland

Accepted 16 November 1984

SUMMARY

1. The anatomy and physiology of neurones underlying escape swimming behaviour in the squat lobster, *Galathea strigosa*, have been investigated, and the results are discussed in the context of the evolution of decapod escape behaviour.

2. In contrast to crayfish, hermit crabs and a number of other related decapods, *Galathea* does not possess a giant fibre system for escape.

3. Fast flexor motor neurones (FFs) and fast extensor motor neurones (FEs) have been shown, by cobalt backfilling, to be homologous with crayfish FFs and FEs in number, size and distribution of somata. A small degree of intersegmental and interspecific variation is noted.

4. The flexor inhibitor (FI) neurone is described in terms of its central anatomy, peripheral function and peripheral branching pattern. In each of these respects the neurone is found to be homologous with the crayfish FI.

5. The neurone homologous with the crayfish motor giant (MoG) in its soma size and position is found to be a typical FF in *Galathea*. This 'MoGH' contrasts with the crayfish MoG in having central neuropilar arborization and in lacking axonal branches in the connectives. These differences can be accounted for by the absence of cord giant axons.

INTRODUCTION

Closely related species may display patterns of behaviour which are basically similar, but differ in detail between species either qualitatively or quantitatively (Tinbergen, 1958, 1960; Berg 1974; Blest, 1960). Such patterns, which have diverged from a common ancestor through different selection pressures in their respective habitats (Baerends, 1958; Wickler, 1961), are termed homologous. In multisegmented animals, basically similar structures may be differentiated and specialized in successive segments, and the types of behaviour in which these structures are used can also differ either qualitatively or quantitatively. Interspecific and intersegmental

* Present address and address for reprints: Department of Physiology, School of Veterinary Science, Park Row, Bristol, BS1 5LS, England.

Key words: Crustacean escape behaviour, homologous motor neurones, giant axons.

differences in homologous patterns of behaviour are reflected in the structure and function of neurones and neural circuits. A determination of the extent and nature of neuronal homology and variation through the comparative study of related segments and species should facilitate an understanding of the processes which underly the development and evolution of neural circuits and of behaviour.

Many decapod crustaceans escape from threats by means of a rapid abdominal flexion, or tailflip. In crayfish, this behaviour is mediated by two pairs of interneurones with giant axons (for recent review see Wine & Krasne, 1982). These make direct electrical connections with a pair of specialized giant motor neurones (the Motor Giants, MoGs) in the connectives between each abdominal ganglion, and indirect weaker connections with a pool of fast flexor motor neurones in each ganglion. During escape the anterior and posterior segments behave differently, depending on the direction of the initiating stimulus. Mittenthal & Wine (1973, 1978) have found that the connections between the giant axons and MoGs are present in some ganglia, but absent in others. In the lobster, escape behaviour does not differ qualitatively from the crayfish, and the giant interneurones and fast flexor motor neurones show apparent strict homology with those of the crayfish (Otzuka, Kravitz & Potter, 1967; Mittenthal & Wine, 1978). In hermit crabs (Crustacea, Anomura) escape behaviour consists of a withdrawal reflex during which they rapidly retract into their shells (Wiersma, 1961; Chapple, 1966). The behaviour is mediated by only one pair of giant axons, thought to be homologous with the crayfish MG axons (Umbach & Lang, 1981); the LG axons appear to be absent in this species. The giant motor neurones (GMs) of the hermit crab are functional homologues of the crayfish MoGs, but their anatomy is significantly different since they synapse with the giant axons close to the ganglionic neuropile. In contrast, the homologous connection in crayfish is located in the connectives near to the exit of the third root (Furshpan & Potter, 1959).

The squat lobster, *Galathea strigosa* (Crustacea, Anomura), differs markedly from both crayfish and hermit crabs. When threatened or startled, it escapes with a series of extension-flexion movements of the abdomen which resemble crayfish tailflips. In contrast to crayfish, however, the abdomen is held flexed beneath the cephalothorax in the stationary animal (Sillar & Heitler, 1982). Thus escape must begin with extension and not flexion. In this paper we examine the anatomy of neurones underlying the escape. The behaviour is not mediated by giant interneurones since these are absent in the abdominal nerve cord. The fast flexor and extensor motor neurones appear homologous with related species. However the neurone homologous with the crayfish MoG is an unspecialized fast flexor. The results, which suggest that escape behaviour is homologous with non-giant swimming in crayfish (Schrameck, 1970), are discussed in the context of the evolution of giant-fibre mediated escape circuits. In the two papers which follow (Sillar & Heitler 1985*a,b*) we have analysed the motor programme for the behaviour, the role of sensory feedback and the mechanisms for burst production in flexor and extensor motor neurones during swimming.

METHODS

Squat lobsters, *Galathea strigosa*, were collected from lobster creels in St Andrews Bay and maintained in circulating sea water aquaria at temperatures ranging from 3

to 15 °C. Mature, healthy adults of either sex, measuring 6–9 cm from tip of rostrum to caudal edge of telson, were used in all experiments.

Anatomy

Relevant parts of the abdominal nervous system were dissected, fixed for 3 h in 3 % phosphate buffered gluteraldehyde and post-fixed in 1 % osmium tetroxide for 30 min. 1-μm sections were stained with Toluidine Blue. The peripheral nervous system of the abdomen was stained with 1 % Methylene Blue (BDH 154490). To examine the central anatomy of extensor and flexor motor neurones, respectively, cobalt chloride (Pitman, Tweedle & Cohen, 1972) was introduced into the cut ends of axons in abdominal 2nd and 3rd roots. On occasions where staining was light, silver intensification was used to enhance cobalt-sulphide stains, using the method of Davis (1982). The following results are based on over 100 such preparations.

Physiology

Conventional methods of extracellular and intracellular recording and display were used throughout. Fast flexor muscle fibres were penetrated using glass microelectrodes filled with 3 mmol l^{-1} potassium acetate and having resistances of 20–40 MΩ. The somata of motor neurones were penetrated in an isolated nerve cord preparation. The nerve cord was pinned ventral side up in a Sylgard-lined Petri-dish and immersed in chilled oxygenated saline (Mulloney & Selverston, 1974, with Tris substituted by TES and buffered to pH 7·2–7·4). The ganglion under study was mechanically desheathed and motor neurone somata were located visually on the basis of soma size and position. Somata were penetrated with glass microelectrodes filled with 5 % Lucifer Yellow (Stewart, 1978) in 1 mol l^{-1} LiCl (40–60 MΩ). Motor neurones were filled using 0·5-s, 10-nA pulses of negative current every second for 20–60 min.

RESULTS

Gross anatomy

The abdominal nervous system in *Galathea* consists of five free abdominal ganglia (G1–G5) linked by paired connectives (Fig. 1C). In crayfish there are six abdominal ganglia. In *Galathea* the first true abdominal ganglion (TAG) has become fused to the posterior end of the thoracic ganglionic mass (TGM). Therefore reference to G1 in *Galathea* corresponds to G2 in crayfish, and so on. Three paired roots arise from each ganglion. As in crayfish and hermit crabs, abdominal third roots (r3) appear to be purely motor and exclusively innervate the flexor muscles. The point of exit of r3 from left and right connectives is asymmetrical; r3 on one side leaves the connective up to 1 mm more rostrally than the other. In addition the third roots of G3 leave the connectives from its dorsal aspect while other abdominal roots arise more laterally (Fig. 1C). These features of abdominal asymmetry and torsion may reflect the close taxonomic relationship between the Galatheid and Pagurid anomurans. However the abdomen of *Galathea* appears to be externally symmetrical (Fig. 1A), and no asymmetries have been observed in either the motor neurone pools or the abdominal musculature.

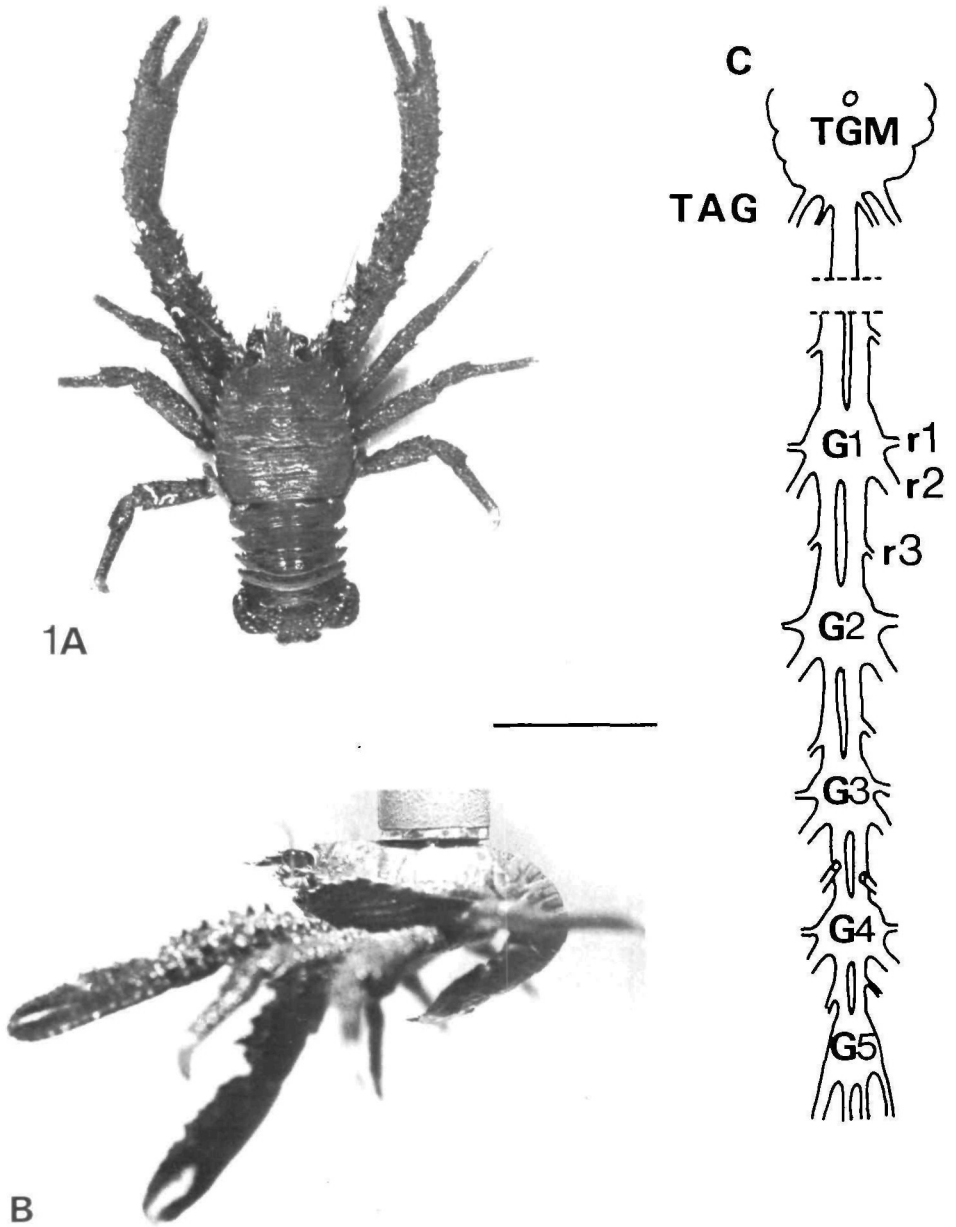

Fig. 1. Anatomy of *Galathea* and its abdominal nerve cord. (A) Dorsal view of *Galathea strigosa* with the abdomen manually extended. Note that the abdomen is externally symmetrical. (B) Lateral view of *Galathea strigosa*. The abdomen is tonically flexed in the resting animal. The animal is suspended from a magnet *via* a small metal plate glued to the dorsal cephalothorax. (C) Schematic representation of the abdominal nerve cord. The five abdominal ganglia (G1–G5) are linked by paired connectives. Above G1 these fuse to form a single nerve cord which enters the first true abdominal ganglion (TAG). TAG is attached to the posterior end of the thoracic ganglionic mass (TGM). The distance between TGM and G1 is up to 20 mm in large specimens. r1, r2, r3 are first, second and third roots, respectively. Note the alternating asymmetry in r3 exit. Scale bar, 4 cm (A, B); 2 mm (C).

Absence of giant axons in the connectives

A striking feature of the abdominal connectives in *Galathea* is an absence of large diameter axons. Cross sections cut at all levels of the abdomen reveal no axon profiles of similar relative diameter to the giant fibres of crayfish or hermit crabs (Fig. 2). In the dorsal region of the connectives just posterior to each ganglion is a group of seven or eight axons which are relatively large in diameter (approx. 20–30 μm) compared with other profiles. In serial sections of the nerve cord these axons leave the connective

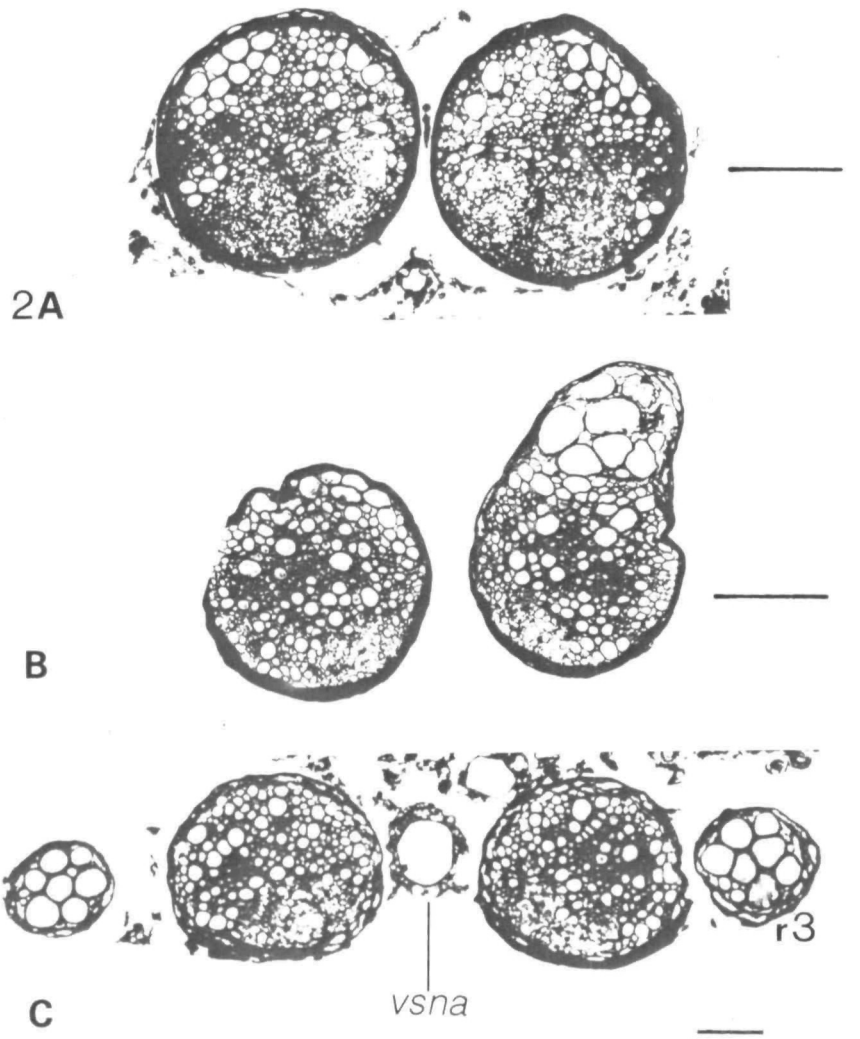

Fig. 2. Cross-sections of the connectives cut at a variety of levels in the abdomen show no giant fibres. (A) Just posterior to G1; (B) between ganglia G3 and G4; (C) just anterior to G5. In (B) r3, containing the FFs, is budding off the right connective, dorsally. In (C) both r3ms, containing the FF axons, lie laterally. *vsna*, ventral subneural artery. Scale bars: A, 100μm; B, 70μm; C, 60μm.

via r3 and are absent in sections cut more posteriorly. Thus, these are the axons of fast flexor motor neurones (FFs). With the exception of these, the dorsal region of the connectives contains a homogeneous population of axon profiles which rarely exceed the diameters of the FFs. In addition, FF axons all have similar diameters, both in the connectives and in r3. This feature also contrasts with crayfish and hermit crabs, in which the axon of the giant motor neurone is significantly larger than other FFs. These results suggest that *Galathea* lacks both giant interneurones and the giant motor neurone although it is likely that homologues of the crayfish neurones are present in reduced form.

Flexor motor neurones

1 mm after leaving the connective, r3 bifurcates into a small superficial branch (r3s) which extends laterally to innervate a thin sheet of ventral tonic flexor muscles, and a larger main branch (r3m) which ascends dorsally and rostrally to innervate the fast flexor muscles. The central anatomy of fast motor neurones has been visualized by selective cobalt backfilling of r3m. Backfilling r3m G2 stains two soma clusters in G2 and one in G3 (Fig. 3). In describing these clusters the terminology of Mittenthal & Wine (1978) for crayfish FFs will be used for ease of comparison. Anterior and contralateral to the filled root is a medial cluster of cells (flexor medial contralateral cluster: FMC) which normally contains four somata. The two largest (approx. 90–110 μm diameter) are homologous with the crayfish F1 and MoG neurones (see below). A second group of neurones have somata located ipsilateral to the filled root in G2 (flexor posterior ipsilateral cluster: FPI). This cluster also contains four somata in G2 with diameters in the range 70–90 μm. Often the FPI neurones form two pairs and the neurites of each pair follow similar paths into the neuropile. A third group (flexor anterior contralateral cluster: FAC), comprising two cells, has somata in the anterior portion of G3 contralateral to the axons.

In terms of the number, size and distribution of somata, FFs in G2 show almost strict homology with crayfish FFs in G3. An exception to this is the occurrence of three FAC FFs in crayfish compared with only two in the homologous cluster in *Galathea*. A further difference is that no branches have been observed arising from any FF axons in the connectives (e.g. Fig. 3A). This contrasts with the crayfish in which the MoG neurone sprouts featherlike processes from its axon near r3, and provides further evidence that *Galathea* may lack a specialized giant motorneurone.

Segmental homology and variation among FFs

The three FF soma clusters have been visualized in G1 to G5 by backfilling r3m of these ganglia (Fig. 4). Attempts to fill r3m to the fused thoracic-abdominal ganglion (TAG) have failed to stain FMC and FPI clusters successfully, probably due to the large distances involved (up to 20 mm in large specimens). However two FAC neurones stain in G1 and eight large axons ascend the connectives towards TAG, suggesting strict homology with G2.

The FAC cluster contains two somata in G1 to G4, but no FAC neurones are present in G5. Each FAC neurone has almost identical anatomy. The axons and neurites of each pair follow similar paths and the two somata are always closely apposed in the anterior contralateral portion of the ganglion.

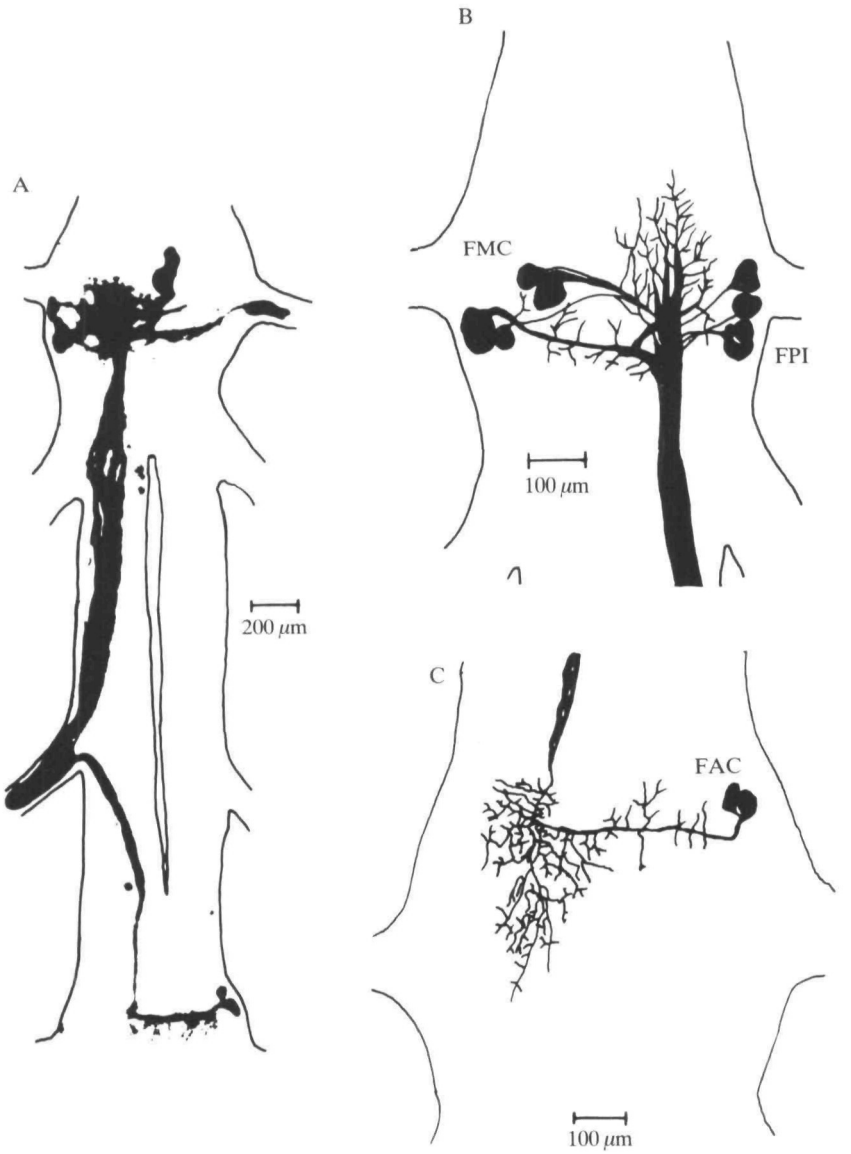

Fig. 3. The central anatomy of fast flexors (FFs) in G2. Backfilling r3m G2 stains three soma clusters. Two are located in G2 and one in G3 (A). In G2 (B) one soma cluster lies contralateral to the filled root (FMC) and comprises four somata. A second soma cluster is located ipsilateral (FPI) and also contains four cells. A third cluster (FAC) comprises two somata which lie in the anterior contralateral portion of G3 (C). (A) is a photograph of a wholemount unintensified backfill. The outline of the nervous system has been added for clarity. B and C are *camera lucida* drawings of wholemount preparations. C is silver-intensified. A, B and C are from different preparations.

The FMC cluster contains four somata in G1 to G3, three in G4 and one in G5. Thus G1, G2 and G3 show strict serial homology in the number, size and distribution of FMC somata. Of the three somata in G4, one is large (approx. 100 μm diameter) and extremely lateral in its location, and is therefore likely to be a homologue of the

B

	Crayfish			*Galathea*			
	FAC	FMC	FPI	FAC	FMC	FPI	
G1	1	4	4	–	(4)	(4)	TAG
G2	3	4	4	2	4	4	G1
G3	3	4	4	2	4	4	G2
G4	2	4	4	2	4	4	G3
G5	0	4	3	2	3	4	G4
G6	–	–	–	0	1	6	G5

Fig. 4.(A) Segmental homology and variation among FPI and FMC fast flexor soma clusters in G1 (i), G2 (ii), G3 (iii), G4 (iv) and G5 (v). G1, G2 and G3 show strict homology. In G4 only three FMC somata stain and no FAC axons descend to G5. G5 deviates most from serial homology with six FPI somata and only one FMC soma. In (v), closed arrows indicate the soma and axon bifurcation of the FMC cell in G5. The open arrow indicates a large unstained soma which may be the contralateral homologue of this cell. Scale bars, 100 μm. (B) Comparison of number and distribution of FFs in abdominal ganglia of crayfish, *Procambarus clarkii* (after Mittenthal & Wine, 1978) and *Galathea*. Dashes indicate lack of data. Numbers in brackets are predicted on the basis of eight ascending axons from fills of r3 TAG.

J. exp. Biol. 117, 237–250 (1985)
Printed in Great Britain © *The Company of Biologists Limited 1985*

MYOCARDIAL OXYGEN CONSUMPTION IN THE SEA RAVEN, *HEMITRIPTERUS AMERICANUS*: THE EFFECTS OF VOLUME LOADING, PRESSURE LOADING AND PROGRESSIVE HYPOXIA

BY A. P. FARRELL*, S. WOOD, T. HART AND W. R. DRIEDZIC

Biology Department, Mount Allison University, Sackville, New Brunswick, Canada, EOA 3CO.

Accepted 29 January 1985

SUMMARY

1. Myocardial oxygen consumption ($\dot{V}_{O_2}$) was measured using an *in situ*, perfused heart preparation at 10 °C. $\dot{V}_{O_2}$ increased in a linear fashion with power output when cardiac output ($\dot{V}b$) was elevated (volume loading). The increased $\dot{V}_{O_2}$ was possible through improved O_2 delivery (increased $\dot{V}b$), but $\triangle P_{O_2}$ (input P_{O_2} − output P_{O_2}) was reduced. The mechanical efficiency of the heart was improved.

2. $\dot{V}_{O_2}$ also increased in a linear fashion with power output when output pressure was increased with $\dot{V}b$ constant (pressure loading). The increased $\dot{V}_{O_2}$ was supported by increased O_2 removal from the perfusate since oxygen delivery ($\dot{V}b$ and input P_{O_2}) was constant. Once more, improved mechanical efficiency was observed.

3. $\dot{V}_{O_2}$ decreased as O_2 delivery was reduced with progressive hypoxia. Even so, power output was maintained at a perfusate input P_{O_2} of 81 Torr. Five of 11 hearts survived a 30-Torr P_{O_2} exposure, but with a 29 % decrease in power output and a 5-fold reduction in $\dot{V}_{O_2}$. The increase in the apparent aerobic efficiency which enabled this is discussed.

INTRODUCTION

Considerable information exists on oxygen uptake ($\dot{V}_{O_2}$) of the mammalian heart, which has a well-developed coronary circulation. In contrast information on $\dot{V}_{O_2}$ of the teleost heart, where coronaries are not always present, is limited. Driedzic, Scott & Farrell (1983) measured myocardial $\dot{V}_{O_2}$ to be about 0·28 $\mu l\,s^{-1}\,kg^{-1}$ fish weight in isolated, perfused sea raven hearts under conditions of low afterload and a reduced cardiac output ($\dot{V}b$). Energy metabolism in the perfused hearts was highly aerobic and $\dot{V}_{O_2}$ increased with power output of the heart.

In view of the modest amount of information concerning myocardial $\dot{V}_{O_2}$, a comprehensive study was initiated using an *in situ*, sea raven heart preparation. The suitability of the preparation for physiological studies is well established (Farrell,

Key words: Myocardium, oxygen consumption, hypoxia.

* Present address: Bioscience Department, Simon Fraser University, Burnaby, B.C., Canada, V5A 1S6.

MacLeod & Driedzic, 1982; Farrell, MacLeod, Driedzic & Wood, 1983), in that the *in situ* heart can generate an *in vivo* work load and the power output of the heart can be varied by simple changes in preload and afterload. The sea raven heart lacks a coronary circulation and so it derives its O_2 supply from venous blood being pumped through the heart. The present work measured myocardial $\dot{V}_{O_2}$ under different power output regimes and different levels of O_2 delivery.

MATERIALS AND METHODS

Animals

Sea ravens, *Hemitripterus americanus* Gmelin, were caught by otter trawl in Passamaquoddy Bay off St Andrews, New Brunswick. The fish were held in aerated, recirculating sea water tanks (9–10 °C) prior to use. A total of 35 fish was used for the study, weighing 0·77–2.05 kg ($\bar{x} = 1{\cdot}25$ kg).

Perfused heart preparation

The *in situ* heart preparation is described in full by Farrell *et al.* (1982, 1983). In essence, the intact heart received a physiological perfusate at a constant input pressure head *via* a cannula placed in the hepatic vein. All other veins entering the sinus venosus were ligated. Cardiac output was delivered against an output pressure head *via* a cannula placed in the ventral aorta. Cardiac output was varied by adjusting the height of the input reservoir (preload). Afterload was varied by adjusting the height of the output pressure head. The nerve supply to the heart was severed and so the intrinsic rhythm of the sino-atrial pacemaker set the heart rate. During the preparation time of 10–15 min, the heart received venous blood or perfusate. The fish was fully immersed in a saline bath which acted as a reference for pressure measurements. The perfusate composition (in mmol l^{-1}) was NaCl, 150; $MgSO_4.7H_2O$, 2; KCl, 5; $CaCl_2$, 2·3; Na_2HPO_4, 2·3; NaH_2PO_4, 0·2; dextrose, 16·7; and 10 g l^{-1} polyvinylpyrrolidone (PVP, $M_r = 40\,000$). Control perfusate was gassed with 0·5 % CO_2 balance air and, after equilibration, the pH was adjusted to pH 7·9 with the addition of $NaHCO_3$ (approximately 10·7 mmol l^{-1}). The perfusate reservoirs, delivery lines, and the saline bath containing the preparation were all water-jacketed to maintain the temperature at 10 °C.

Protocols

Control conditions

Following the cannulation procedures, $\dot{V}b$ and mean output pressure were set at approximately 11 ml min^{-1} kg^{-1} fish weight and 40 cmH_2O, respectively. The heart performed under these conditions for 10–20 min. If $\dot{V}b$ did not stabilize during this period, the preparation was discarded. Representative traces of the control cardiovascular variables ($\dot{V}b$, heart rate, output pressure and input pressure) were collected at the end of this stabilization period. Input perfusate samples were taken from the reservoir to provide three consistent P_{O_2} values. Likewise, the perfusate leaving the ventral aorta was sampled *via* a three-way tap to obtain two consistent P_{O_2} values. ΔP_{O_2} was the difference between the input and output P_{O_2}.

Volume loading

These experiments ($N = 9$ fish) examined the effect of changing power output of the heart while changing O_2 delivery to the heart. Control $\dot{V}b$ was altered by changing preload; power output and O_2 delivery therefore changed in proportion to $\dot{V}b$ since the output pressure head and the perfusate P_{O_2} were unchanged. Three changes in $\dot{V}b$ were examined: control $\dot{V}b$ plus 40 %, control $\dot{V}b$ plus 60 % and control $\dot{V}b$ less 40 %. A 3-min stabilization period was allowed at each new level prior to sampling the output perfusate and the cardiovascular variables. Control conditions were restored for at least 3 min between each challenge and cardiovascular and perfusate samples were taken at the end of each control period.

Pressure loading

These experiments ($N = 15$ fish) examined the effect of changing power output of the heart while maintaining oxygen delivery ($\dot{V}b$ and P_{O_2} constant). Mean output pressure was varied to alter power output, and preload was left unchanged. At each new level, a 3-min stabilization period preceded the sampling of the cardiovascular variables and the output perfusate. Output pressures of approximately 35, 40, 50 and 55 cmH_2O were used. While these pressures span the physiological range for ventral aortic pressures, the net effect on power was small in comparison with the $\dot{V}b$ changes. Control conditions were restored for at least 3 min between each challenge, and samples were taken at the end of this control period.

Progressive hypoxia

These experiments ($N = 11$ fish) examined the effects of a stepwise reduction in the perfusate P_{O_2} with constant preload and afterload. In addition to the control (air saturated) perfusate four other P_{O_2} levels were examined: 105, 80, 55 and 30 Torr. The P_{O_2} of the perfusate was constant. At each new level of hypoxia a stabilization period of 8–10 min was allowed prior to simultaneous sampling of the cardiovascular variables, the input P_{O_2} and the output P_{O_2}. If the cardiovascular variables began to decline abnormally fast at any level of hypoxia, the heart was assumed to be dying and the experiment was stopped. In the hearts that survived the 30 Torr P_{O_2} exposure, preload was increased to evoke the maximal increase in $\dot{V}b$.

Instrumentation

Cardiac output was measured in the outflow line with a flowthrough electromagnetic flow probe and its associated BL 610 Biotronix flowmeter. Input and output pressures were monitored *via* saline-filled cannulae with a Micron pressure transducer (Narco Life Sciences, Houston, Texas). The flow and pressure signals were suitably amplified and displayed on a chart recorder (Biotronix BL 882, Kensington, Maryland). The P_{O_2} of the perfusate was measured at 10 °C with an IL 113 acid-base analyser with associated P_{O_2} electrode and water jacket. The electrode was calibrated with water-saturated gases (100 % N_2 and 12 % O_2) prior to each experiment and the calibration was rechecked with air prior to each sample. The hypoxic gas mixtures

Table 1. *Cardiac variables for control conditions in the different experiments*

	Heart rate (beats min^{-1})	$\dot{V}_b$ (ml min^{-1} kg^{-1})	Mean pressure (cmH_2O)	Power (mW g^{-1})	ΔP_{O_2} (Torr)	$\dot{V}_{O_2}$ (μl s^{-1} g^{-1})	Efficiency (%)	Fish weight (kg)	Ventricular weight (g)
Volume loading ($N = 9$)	40·8 ± 1·4	10·6 ± 0·6	38·6 ± 0·5	1·08 ± 0·09	23·2 ± 1·4	0·316 ± 0·031	16·2 ± 1·0	1·13 ± 0·07	0·86 ± 0·06
Pressure loading (winter) ($N = 9$)	38·8 ± 1·8	11·6 ± 0·6	40·5 ± 0·3	1·21 ± 0·09	23·6 ± 1·0	0·365 ± 0·024	16·5 ± 0·8	1·20 ± 0·09	0·78 ± 0·09
Presure loading (summer) ($N = 9$)	47·8 ± 2·8	10·9 ± 0·4	40·7 ± 0·2	1·06 ± 0·12	31·3 ± 1·9	0·420 ± 0·027	12·4 ± 0·7	1·34 ± 0·11	0·95 ± 0·14
Hypoxia ($N = 11$)	39·2 ± 1·9	11·4 ± 0·3	43·8 ± 0·4	0·95 ± 0·05	24·1 ± 0·6	0·282 ± 0·017	16·9 ± 0·5	1·34 ± 0·15	1·14 ± 0·15

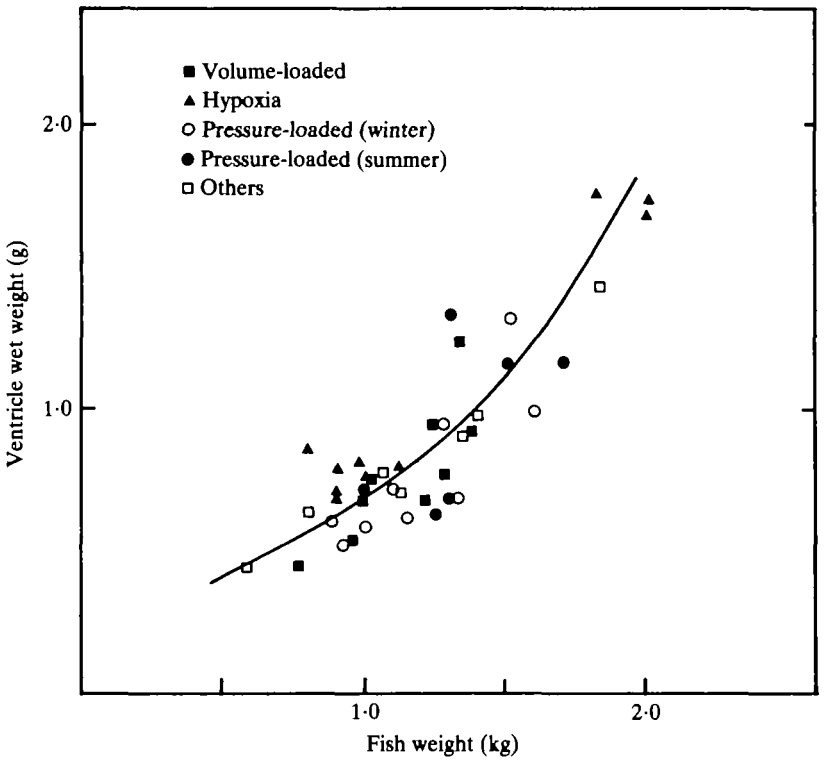

Fig. 1. The relationship between ventricular wet weight and fish body weight. The experiment in which each heart was used is indicated. The line was fitted by eye.

were obtained using a multiple flow controller (Matheson model 8249, East Rutherford, New Jersey).

Calculations

Mean values for input and output pressures and $\dot{V}b$ were obtained from area determinations on the pulsatile traces. The pressures were referenced to the saline level in the chamber and appropriate corrections were made for the pressure drops across the input and output cannulae. All pressures are expressed in cmH_2O (1 cmH_2O = 0·098 kPa). Heart rate was determined from the periodicity of the flow trace. Cardiac output ($ml\,min^{-1}$) = heart rate × stroke volume. Power output of the heart (mW) = (mean output pressure − mean input pressure) × $\dot{V}b$ × (980/60) × 10^{-4}. Oxygen uptake of the heart ($\mu l\,O_2\,s^{-1}$) = ($\dot{V}b/60$) × ($\alpha/760$) × (ΔP_{O_2}) × 10^3, where α = 0·038 ml $O_2\,ml^{-1}\,Torr^{-1}$ partial pressure (Altman & Dittmer, 1971). Mechanical efficiency of the heart (%) = [100] [power (mW) × 0·0498]/[$\dot{V}_{O_2}$ ($\mu l\,O_2\,s^{-1}$)]. Cardiac output was normalized per kg fish weight, and power output and $\dot{V}_{O_2}$ were normalized per g ventricular wet weight. The fish was weighed prior to the experiment and the ventricle was weighed following each experiment (Fig. 1). Each fish acted as its own control and mean values ± S.E. are given where appropriate. Statistical differences ($P < 0·05$) were determined with either a Wilcoxon signed-rank test or a Student's *t*-test.

RESULTS

The control values for the cardiovascular performance and O_2 consumption show good agreement between the three experimental protocols (Table 1). All the experiments were performed during winter months (November–February), except six pressure loading and three volume loading experiments which were performed in early summer (May–June). The summer pressure loading experiments were treated separately in Table 1 since they had a significantly higher intrinsic heart rate, a higher $\dot{V}_{O_2}$ and lower efficiency compared to the winter experiments. There were also small variations in ventricular weight expressed as a percentage of total body weight (Fig. 1).

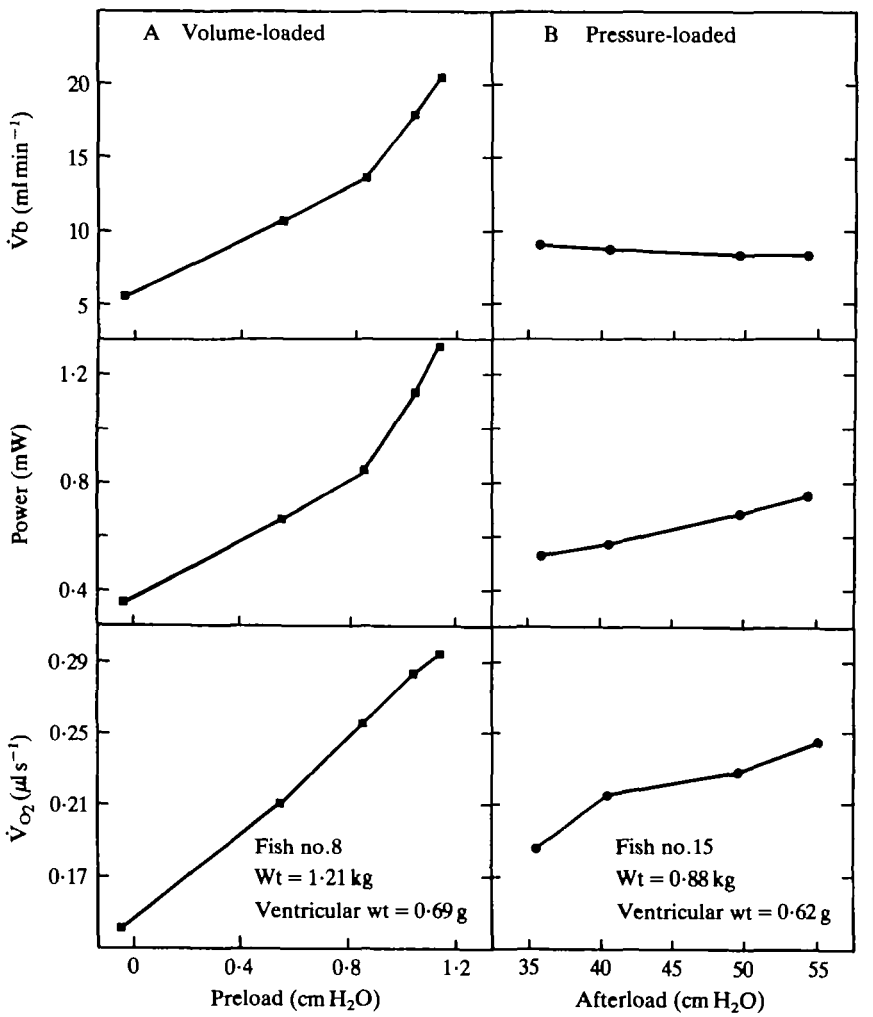

Fig. 2. Cardiac variables [power, oxygen uptake ($\dot{V}_{O_2}$) and cardiac output ($\dot{V}b$)] for individual fish during volume loading (A) and pressure loading (B). Preload was varied in volume-loaded hearts to increase $\dot{V}b$ and power. In pressure-loaded hearts, afterload was varied over a physiological range to increase power with a minimal effect on $\dot{V}b$. Note that physiological changes in $\dot{V}b$ had a far greater effect on myocardial power than physiological changes in afterload.

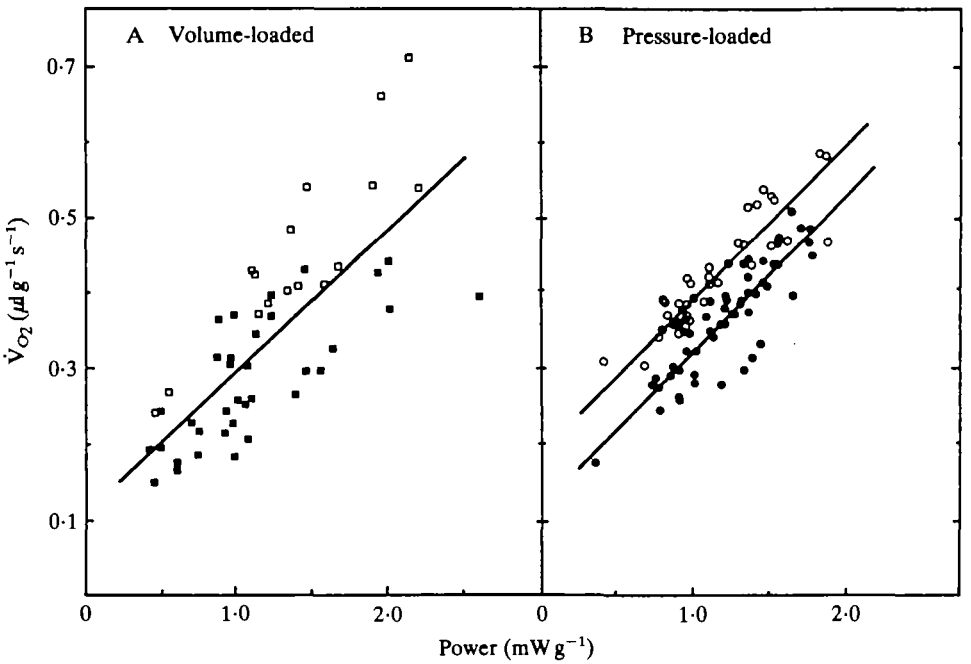

Fig. 3. The relationship between myocardial power output and myocardial oxygen consumption, $\dot{V}_{O_2}$, for volume-loaded (A) and pressure-loaded (B) hearts. Winter experiments (solid symbols) are distinguished from summer experiments (open symbols). For values of linear correlations, see text.

Therefore, the control power output per g ventricle wet weight varied amongst preparations because $\dot{V}b$ was set according to body weight .

Using these data, the average $\dot{V}_{O_2}$ is 0·25 μl s^{-1} for a 1-kg sea raven generating a myocardial power output of 0·85 mW at 10 °C.

Volume loading

An increase in preload produced increases in $\dot{V}b$, $\dot{V}_{O_2}$ and power output (Fig. 2A). All individual fish showed a significant linear correlation between $\dot{V}_{O_2}$ and power output ($r > 93$ % in all nine fish). $\dot{V}_{O_2}$ was linearly related to power output (Fig. 3A), where $\dot{V}_{O_2} = 0{\cdot}188 \times \text{power} + 0{\cdot}110$ ($r = 75{\cdot}9$ %, 50 df, $P < 0{\cdot}05$).

Mechanical efficiency of the heart increased with volume loading. For example, a three-fold increase in power output (0·8 to 2·4 mW g^{-1}) improved efficiency from 15·3 % to 21·3 % (Table 2).

For the $\dot{V}b$ range used in these experiments, ΔP_{O_2} decreased with increases in $\dot{V}b$ (Fig. 4A). Thus, when power output was increased by increasing $\dot{V}b$, there was an increase in $\dot{V}_{O_2}$, an increase in mechanical efficiency, an increase in oxygen delivery, and a decrease in oxygen removal from the perfusate.

Pressure loading

Changes in afterload altered power output without major changes in $\dot{V}b$ (Fig. 2B). Overall, a linear relationship existed between the $\dot{V}_{O_2}$ and power output (Fig. 3B).

Table 2. *Regression equations for $\dot{V}_{O_2}$ and power output: a comparison of normalized data and absolute values*

		Gradient	Intercept	r^2	df	Mechanical efficiency 0·8 mW	2·4 mW
Volume-loaded	normalized*	0·188	0·110	57·6	50	15·3	21·3
	absolute	0·174	0·101	74·1	50	16·6	23·1
Winter pressure-loaded	normalized	0·205	0·120	73·0	50	14·0	19·2
	absolute	0·251	0·049	65·3	50	16·0	18·4
Summer pressure-loaded	normalized	0·204	0·192	84·3	38	11·2	17·5
	absolute	0·333	0·058	61·7	38	12·3	13·9

* Normalized to g ventricular wet weight. Average ventricular wet weights are presented in Table 1.

Since the winter experiments ($N = 9$) differed the summer experiments ($N = 6$), two linear regressions are presented: winter $\dot{V}_{O_2} = 0{\cdot}205 \times \text{power} + 0{\cdot}120$ ($r = 85{\cdot}4\,\%$, 50 df, $P < 0{\cdot}05$) and summer $\dot{V}_{O_2} = 0{\cdot}204 \times \text{power} + 0{\cdot}192$ ($r = 91{\cdot}8\,\%$, 38 df, $P < 0{\cdot}05$). Thus for the summer experiments, $\dot{V}_{O_2}$ was slightly higher for a given power output, i.e. efficiency was lower, but both data sets had the same gradient.

Mechanical efficiency increased with pressure loading. For example, a three-fold increase in power output (0·8 to 2·4 mW g^{-1}) improved efficiency from 10·0 % to 19·2 % and from 11·2 % to 17·5 % in winter and summer experiments, respectively (Table 2).

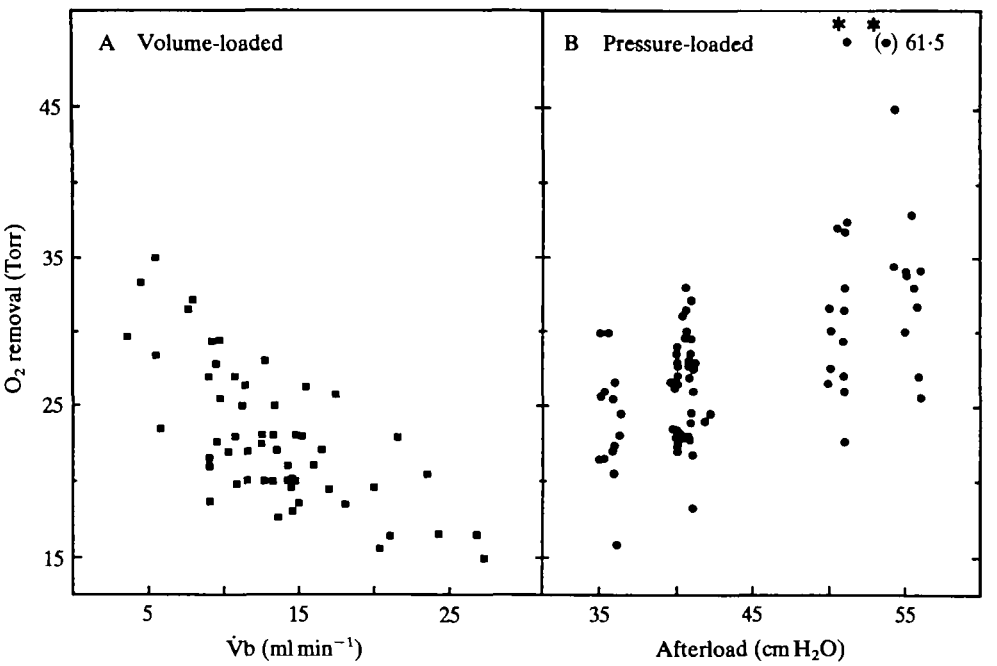

Fig. 4. Scatter diagrams to represent the relationship between O_2 removal from the perfusate (input P_{O_2} − output P_{O_2}) and cardiac output ($\dot{V}b$) in volume-loaded hearts (A) and afterload in pressure-loaded hearts (B). * Denotes that $\dot{V}b$ was not maintained during pressure loading.

ΔP_{O_2} increased with pressure loading in order to meet the added O_2 demand, provided $\dot{V}b$ (i.e. O_2 delivery) was constant (Fig. 4B). Whenever $\dot{V}b$ decreased during pressure loading, P_{O_2} increased markedly. This was particularly evident in the three experiments where a mean output pressure could not be increased to 55 cmH_2O and $\dot{V}b$ decreased as output pressure was raised beyond 50 cmH_2O (Fig. 4B). Here the reduction in O_2 delivery was not completely offset by the increase in O_2 extraction. Control conditions could be restored subsequently, indicating that the heart may not have been damaged by this challenge.

Thus, when power output is increased with a constant O_2 delivery ($\dot{V}b$ and input P_{O_2} constant), an increase in $\dot{V}_{O_2}$ is achieved through improved O_2 removal from the perfusate.

Progressive hypoxia

These experiments lasted up to 80 min. At each level of hypoxia the cardiovascular variables were stable for many minutes and so the data summarized in Fig. 5 apply to relatively steady-state conditions.

Power output and $\dot{V}b$ were not significantly different from their control levels at an input P_{O_2} of 81 Torr, but $\dot{V}_{O_2}$ was significantly reduced (Fig. 5). Maintenance of power output in association with a decrease in $\dot{V}_{O_2}$ resulted in an increase in the apparent aerobic efficiency of the heart. Below an input P_{O_2} of 81 Torr, power output and $\dot{V}b$ were reduced significantly, even though preload and afterload were unchanged. One heart died during the transition from 81 Torr to 55 Torr and five hearts died during the transition from 55 Torr to 30 Torr.

$\dot{V}_{O_2}$ was reduced almost three-fold at 55 Torr and over five-fold at 30 Torr, yet the decreases in power output were small by comparison (81 % and 72 % of control, respectively). At these extremes of hypoxia there was an increase in the apparent aerobic efficiency of the heart.

The intrinsic heart rate ($39{\cdot}8 \pm 1{\cdot}9$ beats min^{-1}) did not change significantly with progressive hypoxia. Heart rate was reduced by 3–5 beats min^{-1} in three of the four hearts that survived at 30 Torr. One additional fish showed an atypical, progressive decrease in heart rate (33·3 beats min^{-1} at 165 Torr to 18·8 beats min^{-1} at 30 Torr, even though $\dot{V}b$, power output, $\dot{V}_{O_2}$ and efficiency were not atypical compared to the other 10 fish.

At a P_{O_2} of 30 Torr, only small increases in $\dot{V}b$ were possible when preload was raised to evoke a maximal increase in $\dot{V}b$. Cardiac output increased by 8 %, 22 %, 46 % and 55 % with no significant change in heart rate in the four fish examined. Such increases in $\dot{V}b$ were terminal in that $\dot{V}b$ decreased rapidly in three of the hearts after only 20–180 s, and the control $\dot{V}b$ could not be restored subsequently. One heart maintained a 22 % increase in $\dot{V}b$ for 10 min without dying.

DISCUSSION

This is the first comprehensive study of myocardial $\dot{V}_{O_2}$ in a teleost. Based on the present observations, myocardial $\dot{V}_{O_2}$ is 0·25 $\mu l\, O_2\, s^{-1}$ for a 1-kg fish with a 0·8-g ventricle generating a power output of 0·85 mW. Driedzic *et al.* (1983), using isolated sea raven hearts, reported a similar $\dot{V}_{O_2}$ value, but the power output was only 0·2 mW

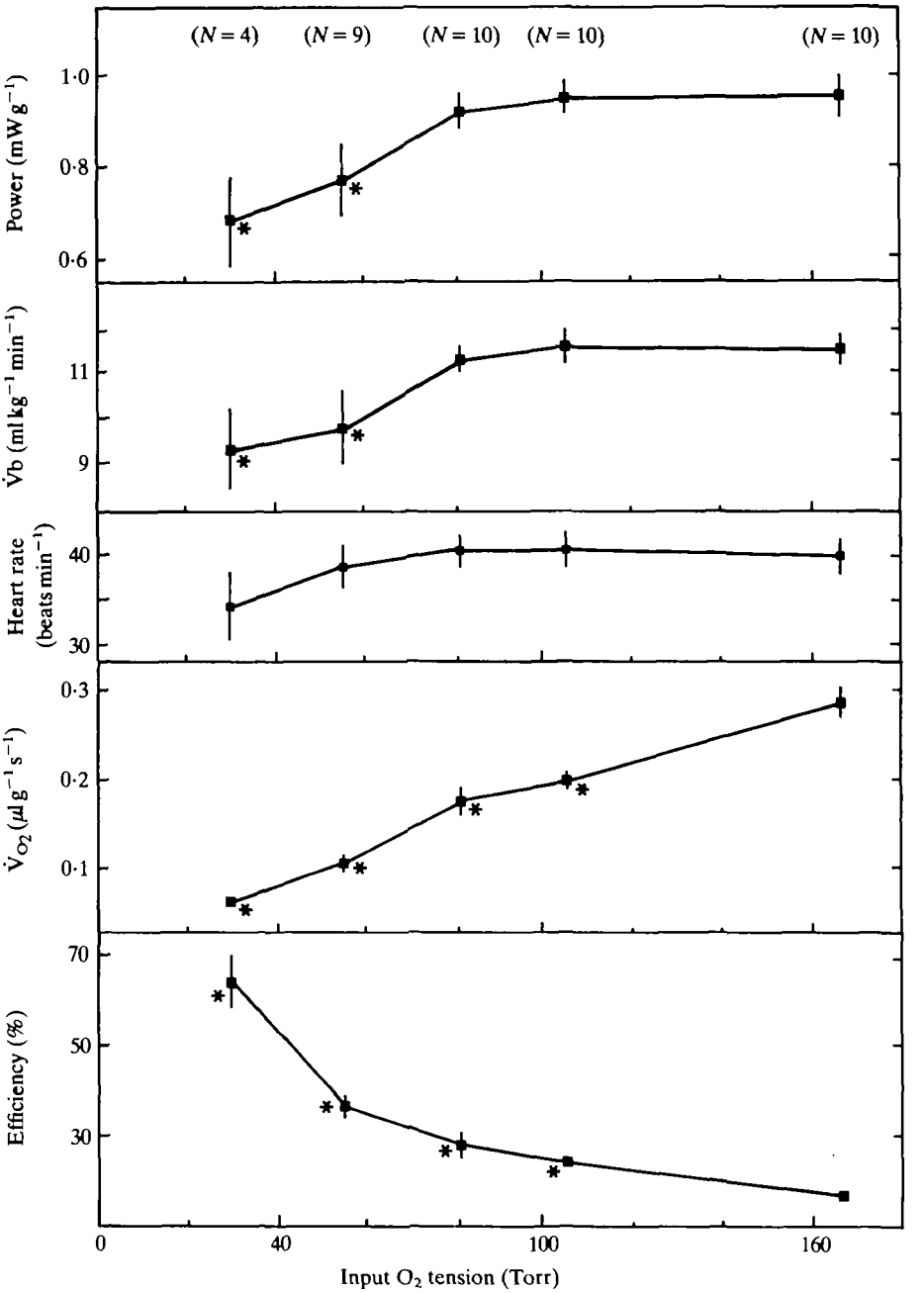

Fig. 5. The effect of four levels of progressive hypoxia on cardiac performance. Each point represents a mean value for N preparations with the standard error indicated by the vertical bar. * Denotes a statistically significant difference from the normoxic control value.

and the mechanical efficiency was 4·2 %. The mechanical efficiency of the *in situ* heart was about 15 %, which is comparable to that of mammalian hearts (rat 11 %, Neely, Liebermeister, Battersby & Morgan, 1967; human 9–11 %, Gibbs & Chapman, 1979). The highest efficiency observed in an *in situ* sea raven heart with normoxic perfusate was 26 %, a value close to the 30 % observed in trained athletes after severe exercise (Gibbs & Chapman, 1979). It seems unlikely that the assumption that the trout heart is 40 % efficient (Jones, 1971) will be substantiated.

The present myocardial $\dot{V}_{O_2}$ measurement can be used to estimate what proportion of the O_2 contained in venous blood is consumed by the heart of the intact fish. Each heart stroke supplies about 10 μl O_2, assuming stroke volume is 0·34 ml kg^{-1} and venous O_2 content is 3 vol%. Yet the myocardium of a 1-kg fish requires about 0·37 μl O_2 per heart beat, assuming heart rate is 40 beats min^{-1}. Thus, myocardial $\dot{V}_{O_2}$ removes less than 4 % of the O_2 available in venous blood. Myocardial $\dot{V}_{O_2}$ is also about 0·6 % of the standard O_2 uptake of the resting animal. This estimate is based on a standard O_2 uptake measurement of 64 μl O_2 s^{-1} kg^{-1} for the lingcod, a fish with a similar lifestyle to the sea raven (Farrell & Daxboeck, 1981), and is in the middle of the theoretical range (0·08 % to 4 %) proposed by Cameron (1975). The above calculations confirm theoretical predictions that the fish heart is efficient (Jones, 1971), has a low metabolic demand in terms of the whole animal (Cameron, 1975), and has a venous O_2 supply that is more than adequate for the myocardial demands of resting fish (Jones & Randall, 1978).

$\dot{V}_{O_2}$ is linearly correlated to power output of the heart and mechanical efficiency is improved as power output is increased. These findings are consistent with observations on mammalian hearts (Neely *et al.* 1967; Gibbs & Chapman, 1979; Suga *et al.* 1981, 1982) but do not support the assumption made for the trout heart (Jones, 1971) that efficiency is constant over a large range of $\dot{V}b$ values.

Using the normalized $\dot{V}_{O_2}$ *versus* power output regression equations, the present findings appear to indicate that pressure work and stroke work have the same metabolic cost in the fish heart. The increases in $\dot{V}_{O_2}$ were equivalent in both pressure-loaded and volume-loaded hearts and efficiency was improved by 5–6 % in both cases when power output was increased three-fold (Table 2). Observations on mammalian hearts demonstrate that an increase in pressure (pressure work) is more costly than an increase in flow (stroke work). Neely *et al.* (1967), for instance, demonstrated that if $\dot{V}b$ was increased three-fold without a significant change in systolic pressure, i.e. diastolic pressure was lowered, heart work increased two- to five-fold without a significant increase in $\dot{V}_{O_2}$. In contrast, $\dot{V}_{O_2}$ increased 65 % with a doubling of heart work when the heart generated a greater aortic pressure and stroke volume was constant. However, when $\dot{V}b$ was increased without regulating systolic pressure (diastolic pressure constant), $\dot{V}_{O_2}$ increased significantly (a two-fold increase for a six-fold increase in heart work). Thus one explanation for the apparently similar metabolic cost of volume and pressure loading in sea raven hearts is that the volume-loaded heart performed additional pressure work as systolic pressure rose with stroke volume (diastolic afterload was unchanged).

The present $\dot{V}_{O_2}$ and power output data were normalized because the animal weight varied substantially (see Neely *et al.* 1967). For the volume-loaded heart, absolute and normalized values give the same relationship between $\dot{V}_{O_2}$ and power output

(Table 2). However, with pressure loading, efficiency does not improve appreciably (1–2 %, Table 2) when absolute values are used, unlike the 5–6 % with normalized values. This difference is probably related to the cost of pressure development in fish of different sizes. Only relatively small changes in power output within individual fish were possible with pressure loading (Fig. 2B) and the maximum power output of the smaller fish did not necessarily overlap with the minimum power output of the larger fish. This separation between the absolute data for large and small fish and the different gradient for $\dot{V}_{O_2}$ *versus* power output, implies that pressure work is more costly in larger fish. This additional cost may be related to the fact that larger fish have relatively larger (thicker?) hearts (Fig. 1).

A seasonal difference in $\dot{V}_{O_2}$ was apparent. Summer fish had a higher $\dot{V}_{O_2}$ and a lower efficiency. Whether this is related to the higher intrinsic heart rate of summer fish observed here and in a separate study (M. S. Graham & A. P. Farrell, in preparation) is not known.

The O_2 content of the air-equilibrated perfusate was 0·76 vol%, which is about four times lower that that of the venous blood supplying O_2 to the heart. Because of this, the P_{O_2} of the perfusate decreases during its passage through the heart, whereas the blood P_{O_2} probably does not change significantly. This raises the question whether O_2 delivery to the myocardium was limited by perfusion with aerated saline. If it is assumed that the *output* P_{O_2} is indicative of the O_2 gradient driving diffusion, then O_2 delivery from aerated perfusate was probably not diffusion limited since the output P_{O_2} (> 130 Torr) of the perfusate was always much greater than the venous P_{O_2} in the intact sea raven (53 Torr, Farrell & Driedzic, 1980). Consequently, the cardiac performance *in situ* is probably directly comparable to the *in vivo* situation despite differences of O_2 content in the perfusion media. This conjecture is also supported by preliminary experiments where oxygenating the perfusate (99·5 % O_2) had no effect on cardiac performance or $\dot{V}_{O_2}$, and by the fact that the *in situ* heart performed physiological workloads and showed no deterioration after 2 h of experiments.

Unlike the situation with aerated perfusate, O_2 diffusion became limiting during perfusion with hypoxic saline. Power output was maintained with an input P_{O_2} of 80 Torr, i.e., when the output P_{O_2} of 60–65 Torr was slightly above the normal venous P_{O_2} of 53 Torr. However, at an input P_{O_2} below 55 Torr (output P_{O_2} of 40–45 Torr) the decrease in O_2 removal as $\dot{V}b$ declined during hypoxia, which is the opposite of the situation with aerated perfusate (Fig. 3A), was a strong indication that O_2 diffusion became limiting. Perhaps the magnitude of the O_2 limitation is better highlighted by the death of some hearts and the poor and often terminal response to preload. Extrapolation of this conclusion to intact fish is restricted by the limited information on the cardiac and venous P_{O_2} during hypoxia. Nevertheless it seems reasonable to assume that O_2 diffusion does become limiting in the intact sea raven at a P_{O_2} perhaps a few Torr lower than that used in the present work: this would account for the negligible change in venous P_{O_2} and the possible importance of facilitated O_2 diffusion by haemoglobin. In other species the limiting P_{O_2} will undoubtedly vary because of myocardial myoglobin content, ventricular thickness and the presence of a coronary circulation. In intact lingcod, a water P_{O_2} of 25–45 Torr reduces cardiac performance ($\dot{V}b$ and arterial pressure reduced by 31 % and 10 % respectively, Farrell 1982), but whether this response reflects an O_2 limitation is

unknown. In contrast, the trout heart, which is supplemented by arterial blood, maintains its performance during environmental hypoxia (P_{O_2} of 40 Torr) when the venous and arterial P_{O_2} levels are 10 and 22 Torr respectively (Holeton & Randall, 1967; Wood & Shelton, 1980).

Hypoxia had no major effect on pacemaker frequency. Any decreases in rate observed here were in unstable preparations exposed to stressful situations (e.g. excessive work loads). These decreases were irreversible. Consequently, the bradycardia observed in intact fish at extremes of environmental hypoxia (e.g. Smith & Jones, 1978; Daxboeck & Holeton, 1978; Wood & Shelton, 1980; Farrell, 1982) is probably entirely a central reflex.

Hearts receiving input perfusate with a P_{O_2} of 80 Torr were able to sustain the same level of performance as control hearts. It has previously been shown that sea raven hearts perfused with air-equilibrated media generate essentially all of their ATP requirements *via* aerobic metabolism (Driedzic *et al.* 1983). Thus, a 1-kg fish, with a 0·8-g heart and an oxygen consumption rate of 0·25 $\mu l\, O_2\, s^{-1}$ would have an ATP turnover rate of approximately 80 nmol ATP $g^{-1}\, s^{-1}$. It may be calculated from the data of Turner & Driedzic (1980) that sea raven hearts subjected to anoxic conditions to stimulate glycolysis have a maximal anaerobic ATP production rate of approximately 20 nmol ATP $g^{-1}\, s^{-1}$. At an input P_{O_2} of 80 Torr, ATP demand could be matched closely with the sum of ATP regeneration through aerobic and anaerobic metabolism. Larger decreases in external oxygen availability resulted in a decrease in performance, presumably due to the inability to increase further the rate of ATP production. Only 5 of 11 hearts withstood the 30 Torr exposure and their capacity to increase $\dot{V}b$ was reduced. Imposed increases in $\dot{V}b$ were also detrimental to the heart's survival. Only one heart sustained an increase in $\dot{V}b$ for longer that 2 min. The rapid collapse of the hearts at high work loads during hypoxia may reflect a problem not only with ATP production but also with the removal of anaerobic end products from the myocardium. Intracellular acidosis is detrimental to cardiac contractility (Gesser & Poupa, 1983; Farrell *et al.* 1983; Farrell, 1984) and it is recognised acidosis combined with anoxia impair contractility of ventricular strips considerably more than anoxia alone (Nielsen & Gesser 1983).

In summary, the present measurements of myocardial $\dot{V}_{O_2}$ under various power output regimes and levels of O_2 delivery indicate many similarities between the fish heart and the mammalian heart despite the anatomical differences and lack of a coronary circulation in the fish. Perhaps the most important difference is the relative tolerance of hypoxia by the fish myocardium. This aspect of myocardial metabolism would be worthy of further investigation.

This work was supported in part by NSERC of Canada through grants to APF and WRD and in part by N.B. Heart Association through a grant to WRD. Appreciation is extended to the Director and staff of the Huntsman Marine Laboratory, St Andrews, N.B. for supplying the animals used in this study.

REFERENCES

ALTMAN, P. L. & DITTMER, D. S. (1971). *Biological Handbooks. Respiration and Circulation*. Federation of American Societies for Experimental Biology, pp. 16–17.

CAMERON, J. N. (1975). Morphometric and flow indicator studies of the teleost heart. *Can. J. Zool.* **53**, 691–698.

DAXBOECK, C. & HOLETON, G. F. (1978). Oxygen receptors in the rainbow trout, *Salmo gairdneri*. *Can. J. Zool.* **56**, 1254–1259.

DRIEDZIC, W. R., SCOTT, D. L. & FARRELL, A. P. (1983). Aerobic and anaerobic contributions to energy metabolism in perfused isolated sea raven (*Hemitripterus americanus*) hearts. *Can. J. Zool.* **61**, 1880–1883.

FARRELL, A. P. (1982). Cardivascular changes in the unanaesthetised lingcod (*Ophiodon elongatus*) during short-term progressive hypoxia and spontaneous activity. *Can. J. Zool.* **60**, 933–941.

FARRELL, A. P. (1984). A review of cardiac performance in the teleost heart: intrinsic and humoral regulation. *Can. J. Zool.* **62**, 523–536.

FARRELL, A. P. & DAXBOECK, C. (1981). Oxygen uptake in the lingcod, *Ophiodon elongatus*, during progressive hypoxia. *Can. J. Zool.* **59**, 1272–1275.

FARRELL, A. P. & DRIEDZIC, W. R. (1980). A comparison of cardiovascular variables in resting eel pout and sea raven. *Mt. Dess. Island Bull.* **20**, 28–30.

FARRELL, A. P., MACLEOD, K. R. & DRIEDZIC, W. R. (1982). The effects of preload, after load and epinephrine on cardiac performance in the sea raven, *Hemitripterus americanus*. *Can. J. Zool.* **60**, 3165–3171.

FARRELL, A. P., MCLEOD, K. R., DRIEDZIC, W. R. & WOOD, S. (1983). Cardiac performance during hypercapnic acidosis in the *in situ*, perfused fish heart. *J. exp. Biol.* **107**, 415–429.

GESSER, H. & POUPA, O. (1983). Acidosis and cardiac muscle contractility: comparative aspects. *Comp. Biochem. Physiol.* **76**, 559–566.

GIBBS, C. L. & CHAPMAN, J. B. (1979). Cardiac energetics. In *Handbook of Physiology*, Vol. 1, Section 2, (ed. R. M. Berne), pp. 775–804. Bethesda, Maryland: American Physiological Society.

HOLETON, G. F. & RANDALL, D. J. (1967). The effect of hypoxia upon the partial pressure of gases in the blood and water afferent and efferent to the gills of rainbow trout. *J. exp. Biol.* **46**, 317–327.

JONES, D. R. (1971). Theoretical analysis of factors which may limit the maximum oxygen uptake of fish: the oxygen cost of the cardiac and branchial pumps. *J. theor. Biol* **32**, 341–349.

JONES, D. R. & RANDALL, D. J. (1978). The respiratory and circulatory systems during exercise. In *Fish Physiology*, Vol. 7, (eds W. S. Hoar & D. J. Randall), pp. 425–501. New York: Academic Press.

NEELY, J. R., LIEBERMEISTER, H., BATTERSBY, E. J. & MORGAN, H. E. (1967). Effect of pressure development on oxygen consumption by isolated rat heart. *Am. J. Physiol.* **212**, 804–814.

NIELSEN, K. E. & GESSER, H. (1983). Effects of $[Ca^{2+}]$ on contractility in the anoxic cardiac muscle of mammal and fish. *Life Sci.* **32**, 1437–1442.

SMITH, F. M. & JONES, D. R. (1978). Localization of receptors causing hypoxic bradycardia in trout (*Salmo gairdneri*). *Can. J. Zool.* **56**, 1260–1265.

SUGA, H., HAYASHI, T., SHIRAHATA, M., SUEHIRE, S. & HISANO, R. (1981). Regression of cardiac oxygen consumption on ventricular pressure-volume area in dog. *Am. J. Physiol.* **240**, H320–H325.

SUGA, H., HISANO, R., HIRATA, S., HAYASHI, T. & NONOMIYA, I. (1982). Mechanism of higher oxygen consumption rate: pressure-loaded vs. volume-loaded heart. *Am. J. Physiol.* **242**, H942–H948.

TURNER, J. D. & DRIEDZIC, W. R. (1980). Mechanical and metabolic response of perfused isolated fish heart to anoxia and acidosis. *Can. J. Zool.* **58**, 886–889.

WOOD, C. M. & SHELTON, G. (1980). The reflex control of heart rate and cardiac output in the rainbow trout: interactive influences of hypoxia, hemorrhage and systemic vasomotor tone. *J. exp. Biol.* **87**, 271–284.

crayfish FI neurone (see below). The remaining two are smaller and anterior in location. Therefore the missing neurone in this cluster may be the homologue of the crayfish MoG neurone. The single FMC neurone in G5 is large (approx. 100 μm diameter) and located near the midline of the ganglion (Fig. 4Av). It is difficult to establish homology with anterior ganglia on the basis of soma position. However the soma can be traced to an axon which bifurcates before exiting *via* r3. This may indicate that the neurone is an FI homologue (see next section).

The FPI cluster contains four somata in G1 to G4 and shows strict serial homology in these ganglia. G5 deviates from strict homology by having six FPI somata. The similarities with crayfish are striking (Fig. 4B). In both species there is a small anterior-posterior reduction in the total number of FFs. In crayfish this has been correlated with a reduction in the flexor muscle mass in caudal segments.

The flexor inhibitor (FI)

In each of G1, G2 and G3 the FMC cluster is strictly homologous with the crayfish in number, size and distribution of somata. The largest and most lateral of these is homologous with the crayfish FI neurone, identified by Wine & Mistick (1977). Cobalt backfilling either r3m or r3s stains the FI soma and an axon which projects

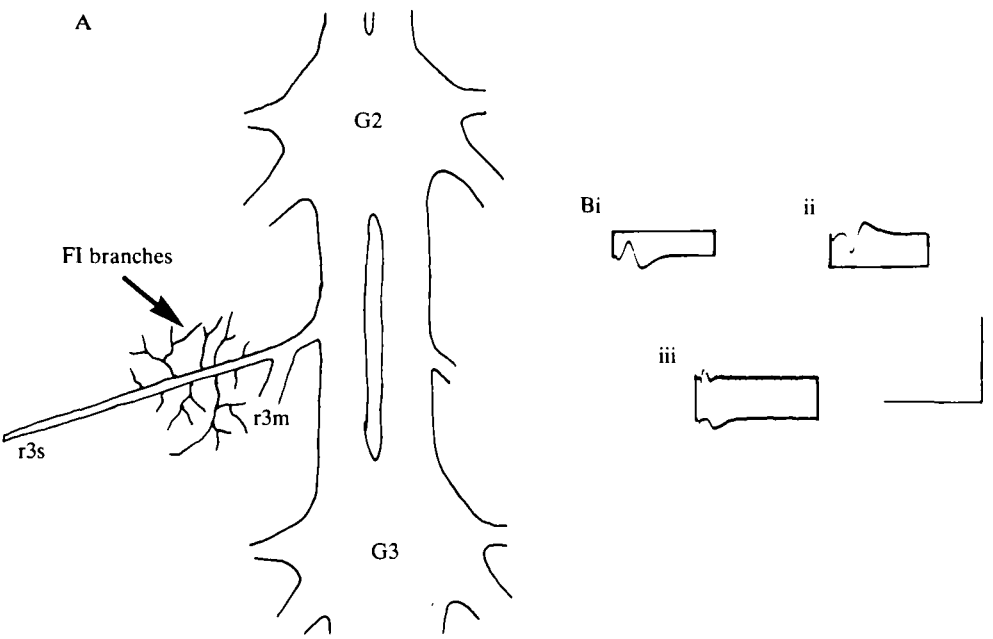

Fig. 5. Anatomical and physiological characterization of FI. (A) Methylene blue stains reveal numerous fine processes arising from the medial portion of r3s and ramifying over the ventral FF muscle fibres. Since FI is the only FF which has an axon branch in r3s, these processes are presumed to belong to FI. (B) Physiological identification of the FI branch point. (i) Stimulating r3s (top trace) results in a short latency spike in r3m (bottom trace) (ii) Stimulating r3m causes a spike in r3s. (iii) Subsequent penetration of ventral FF muscle fibres (in the region depicted in A) results in records showing an IJP (bottom trace, intracellular) correlated 1 : 1 with the spike recorded in r3s (top trace). In this record the FF muscle fibre was depolarized with a holding current of 10 nA. Arrow in A represents region of penetration. Sweeps triggered by stimulus artefact. Scale bars: horizontal, 10 ms (i, ii), 20 ms (iii); vertical, 50 mV (iii).

down the remaining unstained branch of r3. Thus this neurone is the only member of the FF pool whose axon branches at the first bifurcation of r3. Its unique peripheral branching pattern has allowed the following unambiguous identification of the neurone's function and the establishment of homology with the crayfish FI.

Physiological identification of the FI branch point has been obtained as follows (Fig. 5). Extracellular stimulation of r3s or r3m G2 results in a short latency spike recorded in the remaining r3 branch (Fig. 5Bi, ii). This potential is elicited at a set threshold of stimulation and further increases in stimulus intensity (up to 100 V) do not alter its amplitude or waveform. Subsequent intracellular penetration of ventral FF muscle fibres in the region depicted in Fig. 5A, give records showing an inhibitory junctional potential (IJP, Fig. 5Biii) which is tightly coupled to the extracellular spike in threshold and latency. The FI IJP is not always visible in intracellular recordings, presumably because its reversal potential lies close to the resting potential of FF muscle fibres (approx. −70 mV). It was found difficult to alter the membrane potential of FF muscle fibres by injection of up to 10 nA current, probably because of their large volume. On several occasions, however, sufficient depolarization of the muscle membrane was achieved to enhance the amplitude of the FI IJP (Fig. 5Biii). It is not clear whether this was possible because of lower electrode resistance or because penetrations were made closer to FI endplates. On a number of other occasions FI IJPs were hyperpolarizing at resting potential. This may have been due to artificial membrane depolarization resulting from the penetration process.

The central branching of FI has been revealed by injection of Lucifer Yellow into its soma in each of G1, G2 and G3 (Fig. 6). The FI soma was located visually on the basis of its size and position. The dendritic field and major dendritic branches of FI are similar in each ganglion. In addition, the central branching of FI closely resembles that of the crayfish homologue (see Fig. 7 in Mittenthal & Wine, 1978), and no major

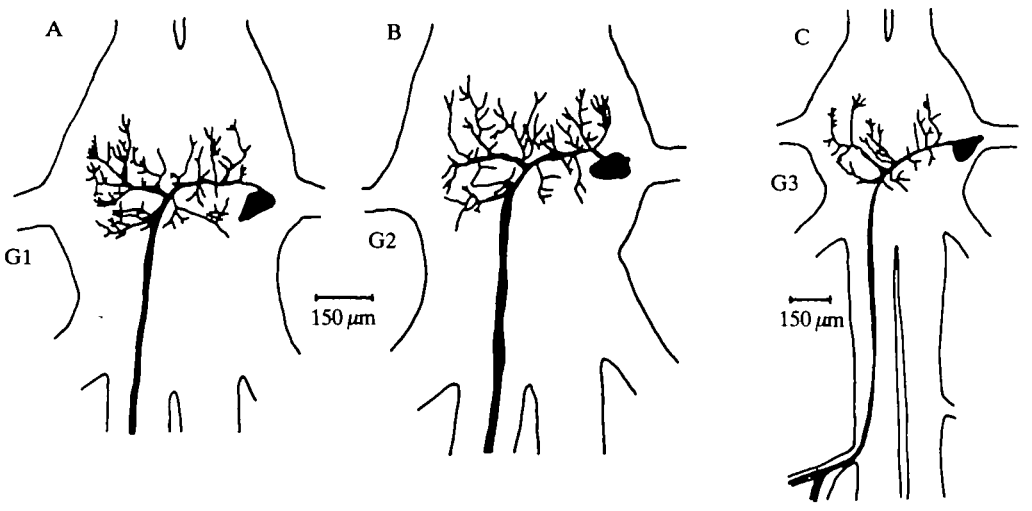

Fig. 6. The central branching of FI in G1 (A), G2 (B) and G3 (C) revealed by injection of Lucifer Yellow. FI has a constant soma position and characteristic central branching pattern. Note in C the FI axon branches at the first bifurcation of r3.

differences exist between the two species. The FI soma is always large (approx. 110 μm diameter) and located at the extreme lateral edge of the ganglion, near the origin of r1. The FI soma often appears ovoid in shape and on some occasions projects partially into the base of the 1st root. This may be due to tissue distortion during processing.

The motor giant homologue (MoGH)

The more medial of the two large FMC somata in G1, G2 and G3 is homologous with the crayfish MoG neurone in terms of its size and position. In contrast to the crayfish MoG, however, this neurone has a complex dendritic tree in the neuropile (Fig. 7A-C) and in this respect appears to be a typical FF. The crayfish MoG has no central dendrites but sprouts featherlike processes in the connectives in the region of the giant fibres (Mittenthal & Wine, 1978). No processes have been observed arising from the MoGH axon in the connectives of *Galathea*. The crayfish MoG branches extensively in the periphery and bifurcates at the first branch point of the third root (Furshpan & Potter, 1959). The MoGH axon in *Galathea* does not branch down r3s but its axon often branches at each bifurcation of r3m suggesting a wide distribution in the periphery.

The crayfish MoG is specialized with respect to the central giants, and receives excitatory input only from them (Wine & Krasne, 1982). In contrast, intrasomatic recordings from the MoGH in *Galathea* reveal a low level of spontaneous synaptic input from a number of unidentified neurones. Single electrical shocks to the TAG–G1 connective elicit a complex compound EPSP in the MoGH soma in G2 (Fig. 8A) in addition to suprathreshold activation of other r3m units. We were unable to observe soma spikes in response to cord stimulation. However, injection of 10 nA

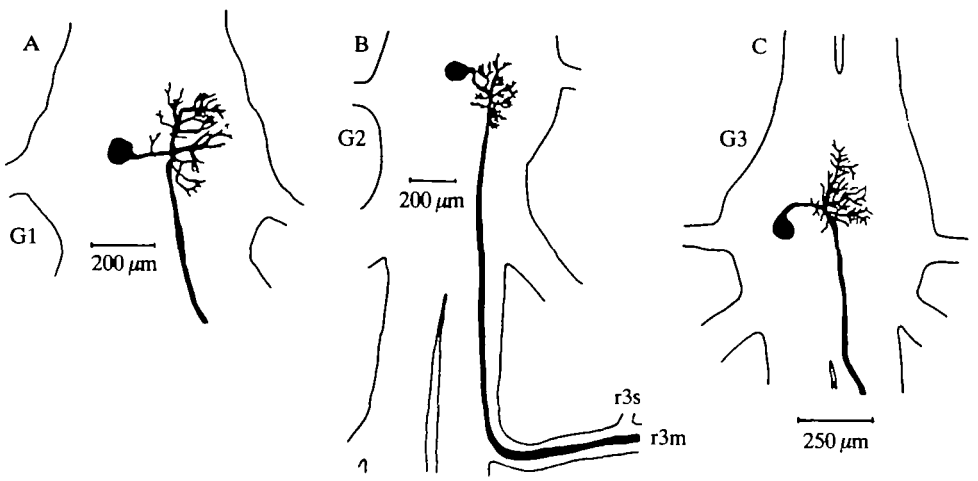

Fig. 7. The central anatomy of MoGH in G1 (A), G2 (B) and G3 (C) following injection of Lucifer Yellow. MoGH arborizes in the main region of flexor neuropile. The MoGH axon has no processes arising in the connectives. It exits *via* r3 and projects down r3m but not r3s (B). In B the MoGH axon branched at the next bifurcation of r3m (not shown).

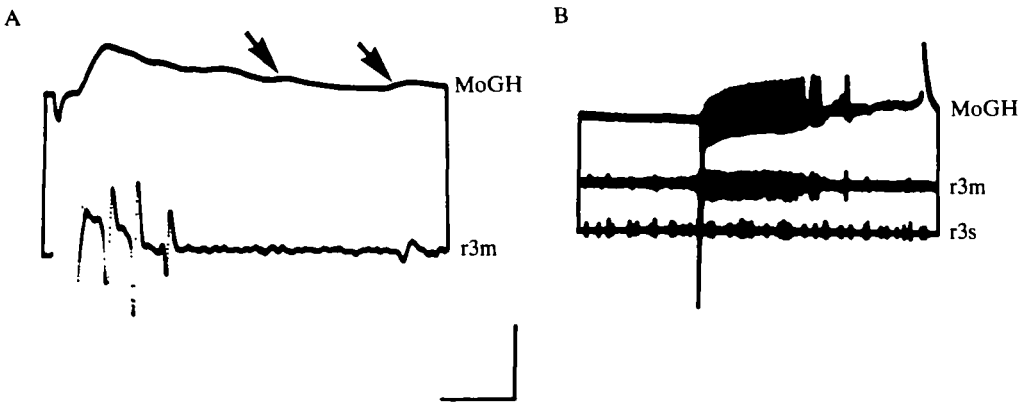

Fig. 8. Physiology of MoGH. The MoGH soma was penetrated in G2. (A) Single electrical shocks (0·5 ms duration) to the TAG–G1 connective elicited a compound EPSP in MoGH (top trace) as well as spiking in a number of other ipsilateral FFs (bottom trace, r3m). Arrows indicate apparent unitary EPSPs. (B) Current injection (+ 10 nA, not monitored) into the MoGH produced a train of soma spikes (top trace) correlated 1 : 1 with spikes recorded extracellularly in r3m (middle trace) but not in r3s (bottom trace). Scale bars: horizontal, 5 ms (A), 250 ms (B); vertical, 5 mV (A), 10 mV (B).

depolarizing current into the soma resulted in a train of spikes which correlated 1 : 1 with spikes recorded extracellularly in r3m (Fig. 8B).

Extensor motor neurones

As in crayfish and lobsters, the axons of efferent and afferent neurones involved in abdominal extension enter the CNS *via* the second root (r2) of abdominal ganglia. Cobalt backfills of r2 G2 stain up to 12 somata in G2 which are distributed among three clusters. Identification of these extensor efferents is based on homologies with neurones in crayfish (Treistman & Remler, 1975; Wine & Hagiwara, 1977) and lobster (Otsuka *et al.* 1967) abdominal ganglia.

As shown in Fig. 9, two clusters of somata are located ipsilateral and one contralateral to the filled root. The somata of four or five fast extensor motor neurones (FEs) form a tight cluster at the ipsilateral edge of the ganglion between the bases of r1 and r2. The diameters of FE somata show considerable variability with a mean of 64 μm. A second cluster lies anterior to the FEs, approximately at the origin of r1, and comprises the somata of four smaller, slow extensor motor neurones (approx. 20–30 μm diameter). In most preparations the neurites of SEs enter the neuropile along a tight tract, distinct from the neurite path of FEs.

In both crayfish (Wine & Hagiwara, 1977) and lobsters (Otsuka *et al.* 1967) the soma of the peripheral inhibitor to the fast extensor muscles (EI) is large (approx. 110 μm diameter in crayfish) and located contralateral to the filled root. Located contralateral to r2 in *Galathea* are two somata (Fig. 9). Of these the largest has a soma diameter of approximately 95 μm; and is therefore labelled the phasic extensor inhibitor (EI). The remaining cell in this cluster has a much smaller soma (approx. 30 μm diameter). In view of its close proximity to EI and its similarity to a small contralateral

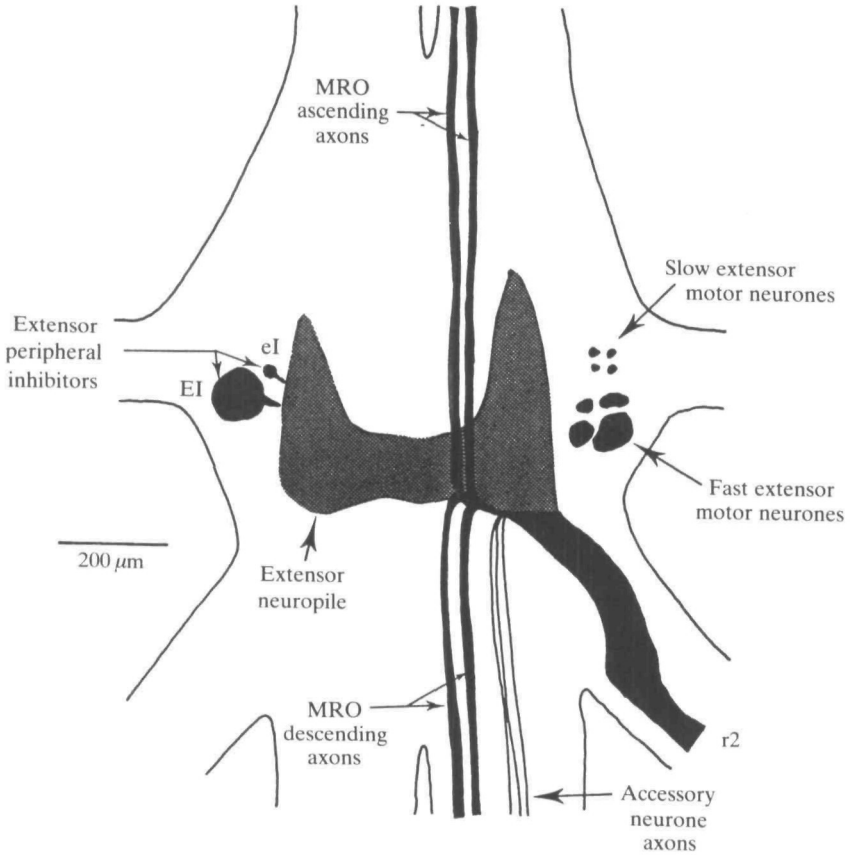

Fig. 9. Overview of extensor efferent somata and MRO axons after a cobalt fill of r2 G2. Stippled area represents the approximate extent of extensor neuropile. Identification of somata is based on a similar overview of crayfish r2 fills (Wine & Hagiwara, 1977).

soma in crayfish this cell is labelled the tonic extensor inhibitor (eI). In crayfish ganglia (Wine & Hagiwara, 1977) a third smaller contralateral soma (approx. 15 μm diameter) of unknown function stains in about 25 % of preparations. In contrast only two contralateral somata are observed in r2 G2 fills in *Galathea*.

The only consistent differences between these results and those of Wine & Hagiwara (1977) for crayfish are the absence of a third contralateral soma and a small reduction in the total number of ipsilateral cells. There are four or five SEs and five or six FEs in crayfish G2. In all essential respects the two pools are homologous in soma size and distribution.

Segmental homologies

Homologous extensor efferents have been stained in each abdominal ganglion except the 5th (last ganglion, not studied) and the fused last thoracic – first abdominal ganglion (Fig. 10). G1, G2 and G3 show strict serial homology in number size and distribution of somata (Fig. 10A–C). In G4, however, there are only three SEs, three FEs and the two contralateral inhibitors (Fig. 10D). This caudal decline in the

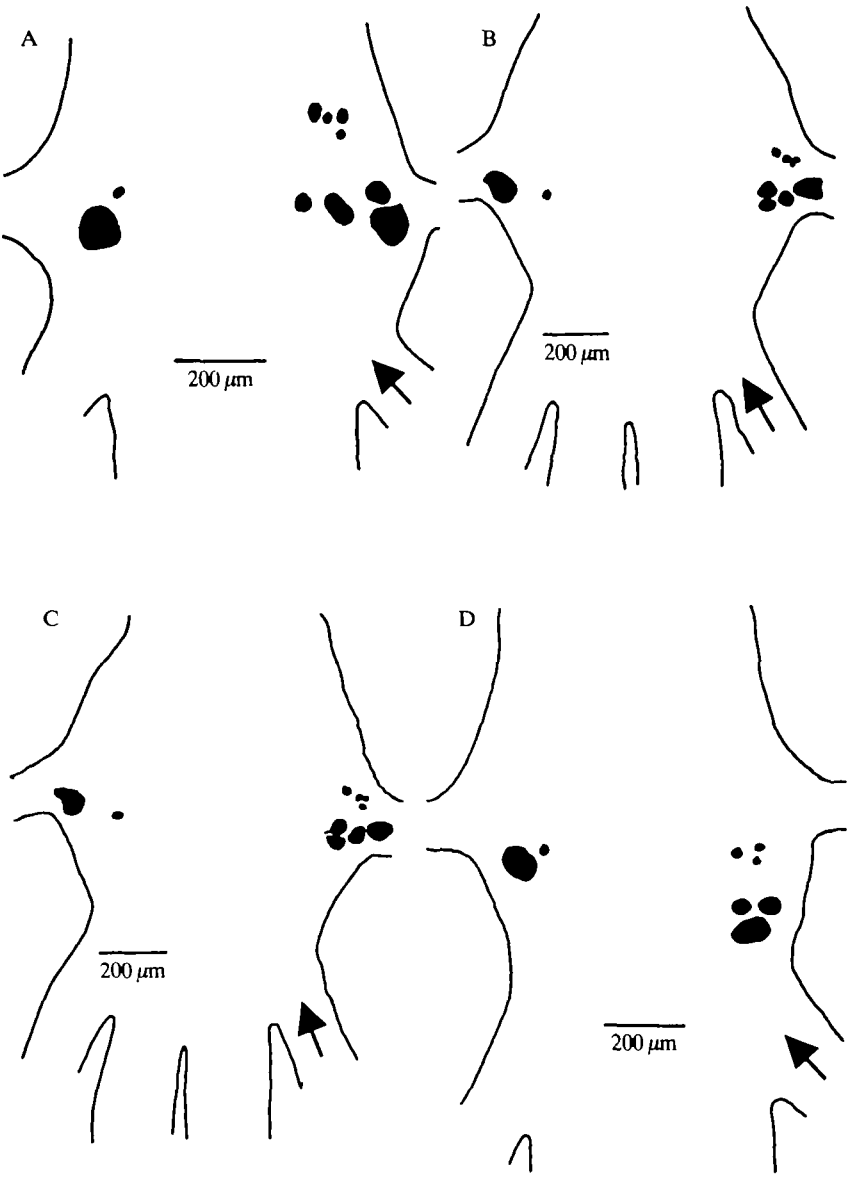

Fig. 10. Segmental homology and variation among extensor efferents in abdominal ganglia G1 (A), G2 (B) and G3 (C) show strict homology in the number, size and distribution of efferent somata, with four FEs, four SEs and two contralateral inhibitors. G4 (D) deviates from strict homology in having only three FEs and three SEs. Arrows indicate roots containing extensor efferent axons. Anterior is at the top.

number of efferent somata is consistent with the result of Wine & Hagiwara (1977) for the penultimate abdominal ganglion in crayfish. TAG also departs slightly from strict serial homology in that only seven ipsilateral and two contralateral somata are stained. Of the ipsilateral cells there are four FEs and three SEs.

Extensor neuropile

The major dendritic domain of the extensor efferents forms a well defined U-shaped region of dorsal neuropile, (Fig. 11), with the densest accumulation of

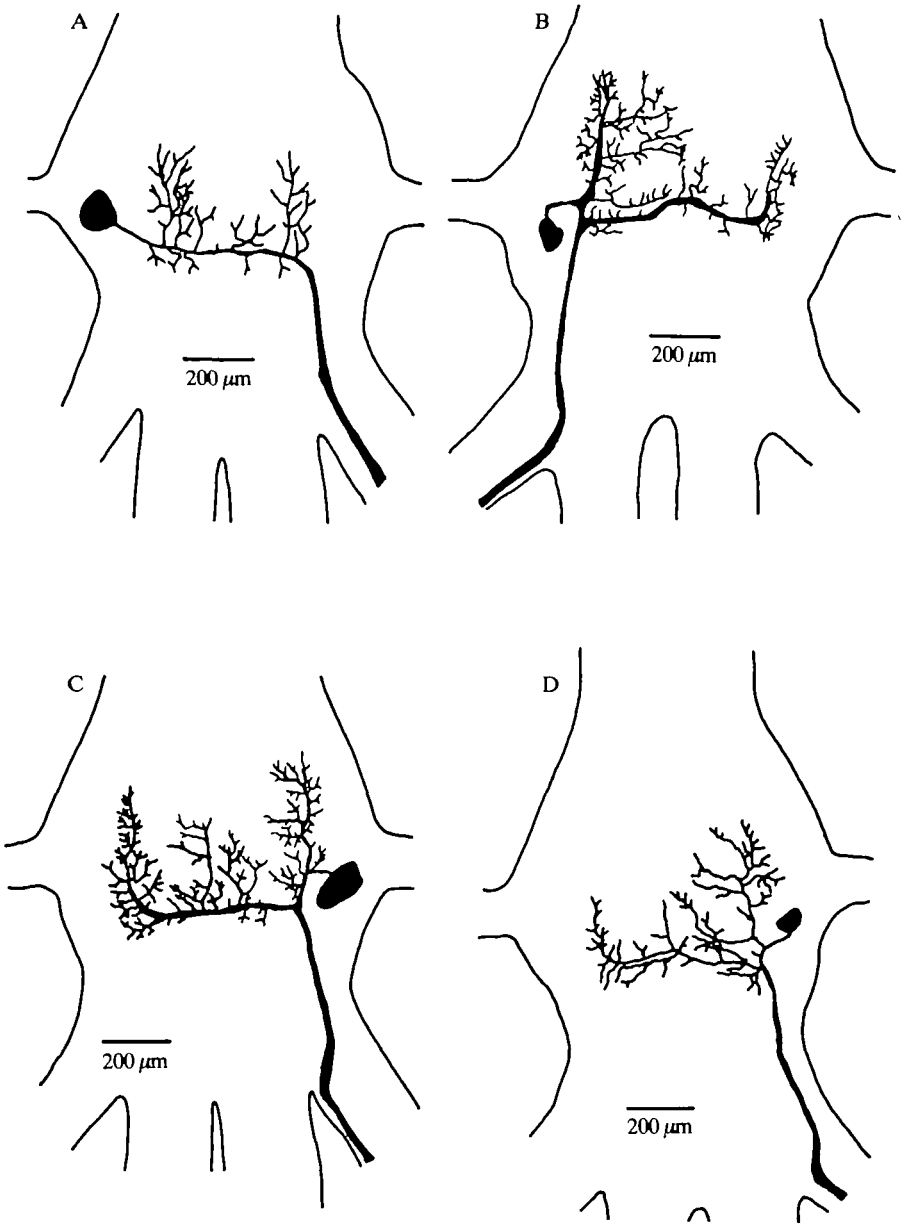

Fig. 11. Central dendritic domains of extensor motor neurones in G2 after intrasomatic injection of Lucifer Yellow. (A) EI has a large contralateral soma and two major regions of dendritic arborization which lie in parallel with the connectives and project rostrally from the neurite. (B)–(D) The FEs all show a similar basic plan in having bilateral dendritic domains.

processes lying on the ipsilateral side of the ganglion. Some of the contralateral neuropilar arborizations can be attributed to EI. When EI is stained selectively by injection of Lucifer Yellow into its soma it is seen to have two major dendritic loci which project anteriorly from the neurite, in line with each contralateral hemiganglion (Fig. 11A). In favourable cobalt fills a tight tract of several large neurites courses horizontally across the ganglion, suggesting that other extensors arborize contralaterally. This has been confirmed by intrasomatic injection of Lucifer Yellow into a number of FEs (Fig. 11B–D). They have complex bilateral branching patterns. The major dendritic branching occurs ipsilateral to the soma but in each fill a large neurite courses laterally across the ganglion to an area of often dense arborization. This feature of FE anatomy contrasts directly with homologous neurones in crayfish (Wine & Hagiwara, 1977), where only a few branches of the extensor excitors may cross the midline of the ganglion.

DISCUSSION

Bullock & Horridge (1965) state that 'Crustacea with a rapid tailflip can be expected to have giant fibres running the length of the cord'. Indeed, among the Crustacea giant fibre systems for escape appear to be widespread, especially amongst those with elongated, flexible abdomens. There are two pairs in *Homarus* (Allen, 1894), *Cambarus* and *Palaemonetes* (Johnson, 1924, 1926) and *Leander* (Holmes, 1942). The stomatopod, *Squilla* has one pair only (Bullock & Horridge, 1965), as do the Anomurans, *Callianassa* (Turner, 1950) and *Pagurus* (Umbach & Lang, 1981). The squat lobster, *Galathea strigosa* (Anomura) has a tonically flexed abdomen at rest (Fig. 1A) which can be repeatedly extended and flexed during escape but it does not possess giant fibres.

In crayfish the giant fibre circuit is now well understood and involves three key neural components: the giant fibres themselves; the MoGs and the Segmental Giants (SGs; Roberts *et al.* 1982). Each of these is thought to be derived from primitive elements in an ancestral non-giant swimming circuit (Wine & Krasne, 1982). Thus it is thought that the giant fibres evolved from smaller premotor interneurones, the MoGs from smaller unspecialized FFs and the SGs from conventional limb motor neurones. The swimming circuit, still present in crayfish, is under the control of a central pattern generator (CPG) which drives extension first with flexion following at short and near constant latency (Reichert & Wine, 1982). Thus the species from which crayfish evolved must have lacked both giant axons in the cord and a pool of MoGs in abdominal ganglia. Moreover escape must have involved backwards swimming by repeated extension-flexion cycles of the abdomen which began with extension. On the basis of the present data, we hypothesize that *Galathea* has features of such an ancestor. If this is so then, in theory at least, each of the three key elements of the crayfish giant fibre circuit will be present in unspecialized or reduced form.

Since the premotor interneurones of the crayfish swimming circuit are numerous, small and largely unidentified (Wine & Krasne, 1982), it may be impossible to identify primitive homologues of the giants in *Galathea* on an anatomical basis. The complete absence of giant fibres in the connectives provides evidence only that escape in *Galathea* involves non-giant circuits. Similarly the SGs probably evolved from

conventional limb motor neurones. The remaining 50 or so swimmeret motor neurones in each hemiganglion are very similar anatomically and hence the search for a primitive SG homologue in *Galathea* is also likely to be unsuccessful.

In contrast, the crayfish MoG was recruited from a relatively small population of large, uniquely identifiable FFs in each ganglion. The MoG differs from other FFs in its soma size and position, location of dendrites and extent of peripheral distribution. Therefore, the primitive homologue of the MoG is identifiable in a non-giant circuit (MoGH).

In terms of the number, size and distribution of FF somata, the homologies that exist between crayfish and *Galathea* are striking (Fig. 4B). In both species anterior ganglia show strict serial and close interspecific homology. In posterior ganglia a decline in the number of FFs occurs and this is correlated in crayfish with an observable reduction in the volume of muscle to be innervated in these segments (Mittenthal & Wine, 1978). The most convincing evidence for homology among FFs in the two species is the FI. This neurone is identifiable on the basis of soma size and position, central branching and peripheral function in *Galathea* and crayfish (Wine & Mistick, 1977). These data imply that the two species derive from a common ancestor and that the FI neurone has changed little since they diverged.

In contrast to FI, the MoGH differs considerably from the crayfish MoG (despite the fact that the two neurones are homologous in soma size and position), having a complex dendritic tree in the neuropile and no axonal branches in the connectives. The major selection pressure on the evolution of the crayfish MoG must have been to ensure a rapid and complete tail flexion in response to a single impulse in the giant fibres. It would seem logical, then, for crayfish to have recruited the largest FF from the available pool (perhaps with the widest peripheral distribution) in order to minimize the amount of modification required in its structure. MoGH in *Galathea* happens to be the largest flexor excitor motor neurone, but other important factors such as axon course and established functional connections with particular premotor elements may well have been important. The possibility that another different FF has assumed the role of MoG in *Galathea* can be ruled out since no axonal specializations have been seen in any FF from cobalt backfills. The FF pools in *Galathea* consist of a homogeneous population of neurones, each with similar anatomy.

The only notable difference that we have observed among FEs in the two species is the presence of strongly bilateral dendritic domains among the fast extensors in *Galathea*. The homologous neurones in crayfish have mainly ipsilateral dendrites with few processes ever crossing the midline of the ganglion (Wine & Hagiwara, 1977).

In crayfish, the presence of ipsilateral FE dendrites has been associated with the retention of a system suitable for independent lateral activity whereas the flexors, with bilateral dendrites (Wine & Hagiwara, 1977), appear specialized to operate bilaterally. But clearly, if *Galathea* does represent the primitive crayfish condition as we have suggested, then the demonstration of bilateral dendrites in this species suggests that crayfish FEs may have secondarily lost their contralateral processes. Crayfish may have evolved lateralized FE dendrites as a concomitant of the giant-fibre system. Post-giant extension in crayfish differs from non-giant extension in being a chain reflex induced by the initial flexion and which is dependent upon patterned sensory feedback

(Reichert, Wine & Hagiwara, 1981). Perhaps it is crucial that post-giant extension is lateralized with respect to this afferent input which may be non-uniform in a changing environment.

Thus several features of escape in *Galathea* resemble the predicted ancestral crayfish form. (1) There are no giant axons in the connectives. (2) The FF and FE pools are homologous with crayfish. (3) The MoGH is an unspecialized FF. (4) Escape involves repeated extension-flexion cycles of the abdomen which begin with extension.

Recent evidence on the escape withdrawal reflex of the hermit crab shows that there is a single pair of giant axons in the connectives which may be homologues of the crayfish medial giant axons. Each central giant axon makes direct electrical connections with a pool of specialized giant motor neurones in the abdomen. These GMs, homologues of the crayfish MoGs, possess most of the anatomical specializations of the crayfish neurone. However, the axonal dendrites are located at the extreme caudal edge of the neuropile and not in the mid-connectives (Umbach & Lang, 1981). Thus the hermit crab lies somewhere between *Galathea* and crayfish in terms of the anatomy of its escape circuitry. The homologies that exist between the FF pools in these three species imply that they all derive from a common ancestor, and that the differences in their escape circuits have resulted from different selection pressures in their respective habitats. The giant fibres of the crayfish are a late development (Wine & Krasne, 1982) and thus unless *Galathea* has secondarily lost the giant fibre-MoG system it must represent an ancestral form in terms of the neural control of abdominal flexion. This means that either the escape system of crayfish and hermit crabs evolved independently but convergently after the divergence of the Macrura and Anomura, or perhaps hermit crabs are more closely related to crayfish than they are to *Galathea*. In either case the non-giant, backward swimming of *Galathea* may represent the primitive form of escape behaviour from which the others evolved.

We wish to thank Mrs C. Lamb for typing the manuscript. This work was supported by an SERC Studentship to KTS and in part by an SERC grant to WJH. We thank W. Stewart for providing a sample of Lucifer Yellow.

REFERENCES

ALLEN, E. J. (1894). Studies on the nervous system of Crustacea. I. Some nerve elements in the embryonic lobster. *Qu. Jl microsc. Sci.* **36**, 461–482.

BAERENDS, G. P. (1958). Comparative methods and the concept of homology in the study of behaviour. *Archs néerl. Zool.* **13**, (Suppl.), 401–417.

BERG, C. J. (1974). A comparative ethological study of strombid gastropods. *Behaviour* **51**, 274–322.

BLEST, A. D. (1960). The evolution, ontogeny and quantitative control of the settling movements of some new world saturniid moths, with some comments on distance communication by honeybees. *Behaviour* **16**, 188–253.

BULLOCK, T. W. & HORRIDGE, G. A. (1965). *Structure and Function in the Nervous Systems of Invertebrates*. San Francisco: W. H. Freeman & Co.

Chapple, W. D. (1966). Asymmetry of the motor system in the hermit crab *Pagurus granosimanus* Stimpson. *J. exp. Biol.* **45**, 65–81.

DAVIS, N. T. (1982). Improved methods for cobalt filling and silver intensification of insect motor neurons. *Stain. Technol.* **57**, 239–244.

FURSHPAN, E. J. & POTTER, D. D. (1959). Transmission at the giant motor synapses of the crayfish. *J. Physiol., Lond.* **145**, 289–325.

HOLMES, W. (1942). The giant myelinated nerve fibres of the prawn. *Phil. Trans. R. Soc. Ser. B.* **231**, 293–311.

JOHNSON, G. E. (1924). Giant nerve fibres in crustaceans with special reference to *Cambarus* and *Palaemonetes*. *J. comp. Neurol.* **36**, 323–373.

JOHNSON, G. E. (1926). Studies on the functions of the giant nerve fibres of crustaceans with special reference to *Cambarus* and *Palaemonetes*. *J. comp. Neurol.* **42**, 19–33.

MITTENTHAL, J. E. & WINE, J. J. (1973). Connectivity patterns of crayfish giant interneurons: visualization of synaptic regions with cobalt dye. *Science, N. Y.* **179**, 182–184.

MITTENTHAL, J. E. & WINE, J. J. (1978). Segmental homology and variation in flexor motorneurons of the crayfish abdomen. *J. comp. Neurol.* **177**, 311–334.

MULLONEY, B. & SELVERSTON, A. I. (1974). Organization of the stomatogastric ganglion of the spiny lobster. I. Neurons driving the lateral teeth. *J. comp. Physiol.* **91**, 1–32.

OTSUKA, M., KRAVITZ, E. A. & POTTER, D. D. (1967). Physiological and chemical architecture of a lobster ganglion with particular reference to gamma-aminobutyrate and glutamate. *J. Neurophysiol.* **30**, 725–752.

PITMAN, R. M., TWEEDLE, C. D. & COHEN, M. J. (1972). Branching of central neurons: intracellular cobalt injection for light and electron microscopy. *Science, N. Y.* **176**, 412–414.

REICHERT, H. & WINE, J. J. (1982). Neural mechanisms for serial order in a stereotyped behaviour sequence. *Nature, Lond.* **296**, 86–87.

REICHERT, H., WINE, J. J. & HAGIWARA, G. (1981). Crayfish escape behaviour: neurobehavioural analysis of phasic extension reveals dual systems for motor control. *J. comp. Physiol.* **142**, 281–294.

ROBERTS, A., KRASNE, F. B., HAGIWARA, G., WINE, J. J. & KRAMER, A. P. (1982). Segmental Giant: evidence for a driver neuron interposed between command and motor neurons in the crayfish escape system. *J. Neurophysiol.* **47**, 761–781.

SCHRAMECK, J. E. (1970). Crayfish swimming: alternating motor output and giant fibre activity. *Science, N. Y.* **169**, 698–700.

SILLAR, K. T. & HEITLER, W. J. (1982). Neural events underlying escape swimming behaviour in the squat lobster, *Galathea strigosa* (Crustacea, Anomura). *Neurosci. Abstr.* **8**, 735.

SILLAR, K. T. & HEITLER, W. J. (1985*a*). The neural basis of escape swimming behaviour in the squat lobster, *Galathea strigosa*. II. The motor programme and sensory feedback interactions *J. exp. Biol.* **117**, 271–289.

SILLAR, K. T. & HEITLER, W. J. (1985*b*). The neural basis of escape swimming behaviour in the squat lobster, *Galathea strigosa*. III. Mechanisms for burst production. *J. exp. Biol.* **117**, 291–306.

STEWART, W. W. (1978). Functional connections between cells as revealed by dye-coupling with a highly fluorescent naphthalimide tracer. *Cell* **14**, 741–759.

TINBERGEN, N. (1958). Comparative studies of the behaviour of gulls (Laridae): A progress report. *Behaviour* **15**, 1–70.

TINBERGEN, N. (1960). The evolution of behaviour in gulls. *Scient. Am.* **203**, 118–130.

TREISTMAN, S. N. & REMLER, M. P. (1975). Extensor motor neurons of the crayfish abdomen. *J. comp. Physiol.* **100**, 85–100.

TURNER, R. S. (1950). Functional anatomy of the giant fibre system of *Callianassa californiensis*. *Physiol. Zoöl.* **23**, 35–41.

UMBACH, J. A. & LANG, F. (1981). Synaptic interaction between the giant interneuron and the giant motor-neuron in the hermit crab, *Pagurus pollicarus*. *Comp. Biochem. Physiol.* **68**A, 49–53.

WICKLER, W. (1961). Okologie und stammesgeschichte von verhaltenswiesen. *Fortschr. Zool.* **13**, 303–365.

WIERSMA, C. A. G. (1961). Reflexes and the central nervous system. In *The Physiology of Crustacea*, Vol. II, (ed. T. H. Waterman), pp. 241–279. New York: Academic Press.

WINE, J. J. & HAGIWARA, G. (1977). Crayfish escape behaviour. I. The structure of efferent and afferent neurons involved in abdominal extension. *J. comp. Physiol.* **121**, 145–172.

WINE, J. J. & KRASNE, F. B. (1982). The cellular organization of crayfish escape behavior. In *The Biology of Crustacea*, Vol. 4, *Neural Integration and Behavior*, (eds D. C. Sandeman & H. L. Atwood), pp. 241–292. New York: Academic Press.

WINE, J. J. & MISTICK, D. C. (1977). Temporal organization of crayfish escape behaviour: delayed recruitment of peripheral inhibition. *J. Neurophysiol.* **40**, 904–925.